

Strategies for Improving the Photocatalytic Hydrogen Evolution Reaction of Carbon Nitride-Based Catalysts

Xueze Chu, C.I. Sathish, Jae-Hun Yang, Xinwei Guan, Xiangwei Zhang, Liang Qiao, Kazunari Domen, Shaobin Wang, Ajayan Vinu,* and Jiabao Yi*

Due to the depletion of fossil fuels and their-related environmental issues, sustainable, clean, and renewable energy is urgently needed to replace fossil fuel as the primary energy resource. Hydrogen is considered as one of the cleanest energies. Among the approaches to hydrogen production, photocatalysis is the most sustainable and renewable solar energy technique. Considering the low cost of fabrication, earth abundance, appropriate bandgap, and high performance, carbon nitride has attracted extensive attention as the catalyst for photocatalytic hydrogen production in the last two decades. In this review, the carbon nitride-based photocatalytic hydrogen production system, including the catalytic mechanism and the strategies for improving the photocatalytic performance is discussed. According to the photocatalytic processes, the strengthened mechanism of carbon nitride-based catalysts is particularly described in terms of boosting the excitation of electrons and holes, suppressing carriers recombination, and enhancing the utilization efficiency of photon-excited electron-hole. Finally, the current trends related to the screening design of superior photocatalytic hydrogen production systems are outlined, and the development direction of carbon nitride for hydrogen production is clarified.

However, as one of the most abundant elements in the universe, hydrogen molecules can be barely found in our atmosphere, and most hydrogen atoms are combined with other elements to form water, carbohydrates, and various organic materials. In order to obtain hydrogen gas, reformation, decomposition, and splitting reactions are the primary hydrogen production methods.^[3] The statistics show that more than 95% of hydrogen gas comes from fossil fuel-based processes like the reformation and decomposition of compounds are still based on fossil fuels and are not sustainable for the future. In comparison, only 3.9% from water-splitting electrolysis, and 0.1% from other sources.^[4-7] There is a huge market for green hydrogen technologies combined with solar energy harvest.^[8,9]

Photocatalysis for water splitting was discovered by Fujishima and Honda in 1972,^[10] providing a way to convert solar energy to chemical energy directly. Since then, extensive efforts have been made to the water splitting technology

for practical applications.^[11-16] However, its development is relatively slow compared to photovoltaic technologies, which have been widely commercialized and applied in various areas. The major hurdle of photocatalysis-based water splitting is its low


1. Introduction

Hydrogen is the only existing fuel that does not release hazardous products and greenhouse gases during its ignition in the air.^[1,2]

X. Chu, C.I. Sathish, J.-H. Yang, X. Guan, X. Zhang, A. Vinu, J. Yi
Global Innovative Center of Advanced Nanomaterials
School of Engineering
College of Engineering
Science and Environment
University of Newcastle
Callaghan, NSW 2308, Australia
E-mail: ajayan.vinu@newcastle.edu.au; jiabao.yi@newcastle.edu.au

L. Qiao
School of Physics
University of Electronic Science and Technology of China
Chengdu 610054, P. R. China

K. Domen
Research Initiative for Supra-Materials Interdisciplinary Cluster for
Cutting Edge Research
Shinshu University
4-17-1, Wakasato, Nagano-shi, Nagano 380-8533, Japan
S. Wang
School of Chemical Engineering and Advanced Materials
The University of Adelaide
Adelaide, SA 5005, Australia

 The ORCID identification number(s) for the author(s) of this article can be found under <https://doi.org/10.1002/smll.202302875>

© 2023 The Authors. Small published by Wiley-VCH GmbH. This is an open access article under the terms of the Creative Commons Attribution License, which permits use, distribution and reproduction in any medium, provided the original work is properly cited.

DOI: 10.1002/smll.202302875

efficiency, which is mainly determined by the quantum efficiency of catalysts.

Photocatalysts, generally semiconductors, are critical for achieving high efficiency of photocatalytic hydrogen evolution.^[17–19] Many semiconducting photocatalysts have been explored for photocatalytic hydrogen evolution reaction (HER).^[20,21] However, the efficiency is still far from the desired performance for several reasons, such as low absorption in the visible light region, low mobility and kinetics of the photogenerated charges, and rapid recombination of electrons and holes. Especially, the new metal-free graphitic carbon nitride (g-C₃N₄) has gained extensive attention.^[22–30] It has shown effective photocatalysis due to an appropriate bandgap, conduction and valence energy level, and environmentally friendly nature.^[31,32] Likewise, exceptional chemical stability, tunable bandgap, photochemical stability, abundance and low cost of resources, biocompatibility, and versatility in composite formation and catalyst design make g-C₃N₄ as a preferable photocatalyst for HER driven by visible light.^[33] Still, the photocatalytic performance of g-C₃N₄ is unsatisfactory because of the lower quantum efficiency, higher recombination of electron–hole pairs, limited visible light absorption ability, and small specific surface area. To date, massive research efforts have been devoted to the development of various g-C₃N₄-based catalysts to resolve the above application defects. For example, incorporating conductive carbon-based materials can enhance the charge transfer kinetics^[34,35] and the heterojunction with other photocatalysts can achieve a synergistic effect on photocatalytic HER due to the enhanced charge transfer and charge separation.^[36–38] Doping of different elements, such as metals or nonmetals including Cu, N, B, O, P, or S, can improve the conductivity, tune the electronic structure and enhance surface functionality, resulting in the promoted performance in HER.^[23,39,40] Additionally, the overlap area between g-CN with other materials provides another opportunity to enhance photocatalytic performance, which promotes the charge transfer between the layers.^[41] This excited state charge transfer is crucial for catalysis, which is not experienced in surface-modified CN sheets. The electronic arrangement of g-CN affects the vibrational coupling patterns, directly affecting vibronic coupling mechanisms in charge transfer.^[42] Furthermore, the control of crystal structure, orientation, defects, and hydrogen and oxygen level in carbon nitride will also strongly influence hydrogen evolution performance.^[43–45]

Although several reviews pertaining to g-CN and their HER applications have previously been published,^[23,46–58] they were rather focused on materials or performance aspects, and no study comprehensively summarized the strategies to improve the performance of photocatalysis toward HER. In this work, we will introduce and discuss the strategy for improving the efficiency of photocatalysis-based water splitting, including bandgap and electronic structure engineering, heterostructure configuration, crystallinity control, structure and defects, and generating active sites by the incorporation of other catalysts and structural engineering. A critical discussion on the state-of-the-art results and the major challenges that need to be addressed are highlighted in order to deliver a viable technology of g-CN-based photocatalysts in the near future.

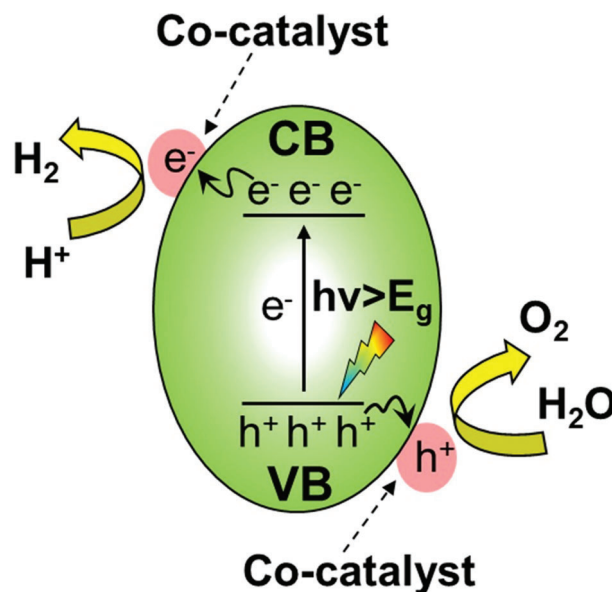


Figure 1. The schematic diagram of carbon nitride-based photocatalytic water splitting.

2. Mechanism of Photocatalytic Water Splitting

As illustrated in **Figure 1**, a carbon nitride-based photocatalytic water-splitting process can be divided into three steps: excitation of electron–hole pairs by light absorption, transportation of the charge carriers to the catalytic sites, and redox reaction for generating the hydrogen and the oxygen. The excitation step is mainly influenced by the electronic band structure of a catalyst. The photocatalyst with a narrow bandgap can generate more amounts of excited electron–hole pairs under the same illumination condition since it can be photoexcited under the light with longer wavelength. After the excitation, hot electrons and holes must migrate to active sites for their utilization. During the transportation process, charge migration can be affected by crystal structures, in which, disordered or defective crystal structures could slow down the charge migration and the recombination of electrons and holes can happen. On the other hand, some special heterostructures can accelerate the charge transport via an internal electric field.^[59] Once electrons and holes reach the active sites, they will be consumed by protons or water to produce hydrogen and oxygen.

In evaluating catalytic performance, the quantum efficiency in photocatalytic hydrogen evolution is the most important factor and criterion, including apparent quantum efficiency (AQE) and internal quantum efficiency (IQE). AQE is calculated as $AQE = \frac{\text{number of reacted electrons}}{\text{number of incident photons}} \times 100\%$, and IQE is calculated as $IQE = \frac{\text{number of reacted electrons}}{\text{number of absorbed photons}} \times 100\%$. The overall efficiency is strongly dependent on AQE. However, the bandgap of g-C₃N₄ is around 2.7 eV, which is close to blue light. Therefore, the quantum efficiency of catalytic performance is relatively low and few works were reported based on the full solar spectrum. A typical example of the reported full solar spectrum quantum efficiency for photocatalytic hydrogen evolution is only 0.588%.^[8] Such low efficiency is not suitable for practical applications.

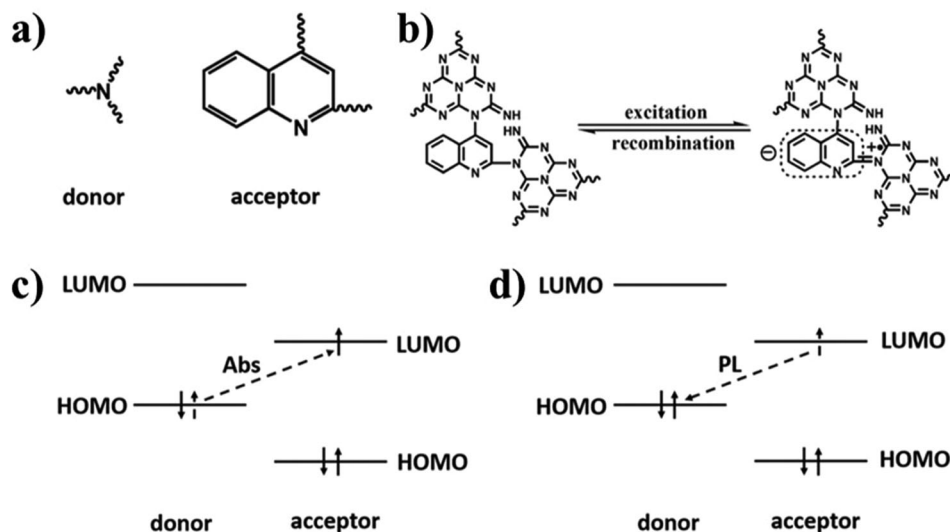


Figure 2. Schematics of a) electron donor and acceptor, b) charge carrier excitation and recombination, c) charge-transfer transition, and d) photoluminescence (PL) path in quinoline-incorporated g-C₃N₄. Reproduced with permission.^[70] Copyright 2015, American Chemical Society.

In this review, we will focus on the process of HER. Pt is the most frequently used water reduction cocatalyst deposited on the catalyst by a photodeposition method, which can be realized by mixing H₂PtCl₆ solution (as a hole scavenger) with the catalyst and followed by illumination. Occasionally, Pd, Au, and non-precious metals are also used as water-reduction co-catalysts. For water oxidation reactions, cocatalysts are typically metal oxides, such as RuO₂, Cr₂O₃, CoO, etc. We will discuss the techniques that can benefit photocatalytic HER using these three steps.

3. Strategies for Improving the Performance of Photocatalytic HER

3.1. Electron–Hole Excitation

3.1.1. Bandgap Engineering

Functional Group Tuning: For increasing the water splitting rate by absorbing more visible light, carbon nitride photocatalyst with a narrower bandgap is desired. There are multiple ways to design the band structure, which can either facilitate or suppress electron–hole excitation. An enlarged bandgap with limited visible light absorption is usually unfavorable, while nanostructuring leads to an enlarged bandgap.^[60–66] In this case, introducing functional groups to carbon nitrides can be a tool for tuning band structure. However, due to the chemical stability of carbon nitrides, functional group tailoring usually occurs in extreme conditions. For example, heptazine heterocycles in carbon nitride sheets can be opened and converted to cyano groups after fluorination with XeF₂ and defluorination at 600 °C in Ar.^[67] The absorption edge of modulated carbon nitride sheets is extended from 420 to 578 nm. Compared with the untreated sample, the hydrogen evolution rate is enhanced by 14.5 times to 3.81 mmol h⁻¹ g⁻¹. The enhanced photocatalytic hydrogen generation performance is mainly ascribed to the narrower bandgap and suppressed charge recombination.^[67] A cyano group can also be introduced via a quick thermal treatment.^[68]

Besides cyano groups, other functional groups, such as carboxyl groups,^[69] can also tune the band structure and extend the absorption band.

As illustrated in **Figure 2**, doped molecules in a carbon nitride framework can behave as electron acceptors, remarkably improving HER activity. Electrons need less energy to be excited from the valence band (VB) to the conduction band (CB). It is different from the electron transfer from VB to CB mechanism of type II heterostructure because building a heterostructure will not change the electron excitation mechanism of a material. We will discuss the mechanism of heterostructure in the following section. Because of the reduced excitation energy, the engineered material is capable of absorbing long-wavelength light, thus benefits photocatalytic activity.^[70,72] It has been shown that various organic molecules with an aromatic structure (**Table 1**), such as benzene,^[73] quinoline,^[70] and pyromellitic dianhydride,^[74] can be doped into the carbon nitride framework to improve the photocatalytic HER activity.^[71]

In the case of doping aromatic molecules into polytriazine imide (PTI), one kind of carbon nitride, the performance enhancement mechanism is similar to that of doped tri-s-triazine-based carbon nitride. This triazine-based carbon nitride, PTI, has a comparable HER rate to that of tri-s-triazine-based carbon nitride. However, the pristine PTI's absorption edge is usually less than 400 nm, suggesting it is inactive to visible light. For extending the absorption edge to a longer wavelength, a small amount of 2,4,6-triaminopyrimidine (TAP) can be added to melamine as a dopant. One doped TAP molecule can provide one nitrogen-vacancy defect to the polymerized carbon nitride (**Figure 3a–d**). The absorption band can be expanded to the visible light region by increasing the defects. The perfect in-plane arrangement and the optimized ratio of pyrimidine and triazine moieties are critical factors that reach an optimum photocatalytic HER activity. Hence, additional pyrimidine moieties in the lattice can suppress photocatalytic activity.^[75,77]

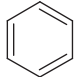
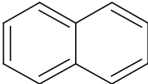
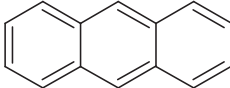
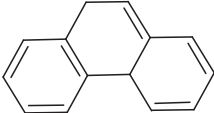

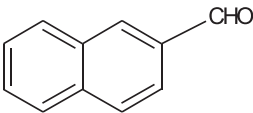
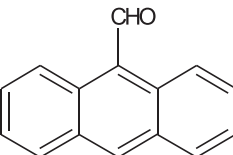
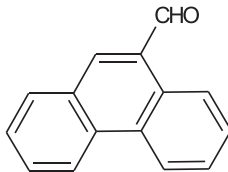
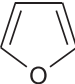
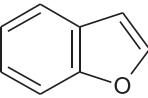
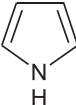
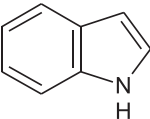
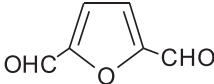
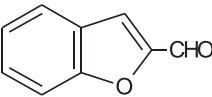
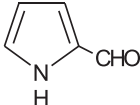
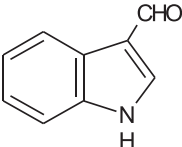
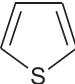
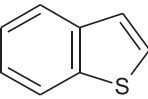
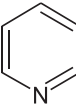
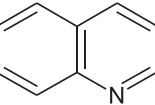
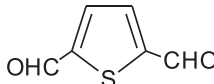
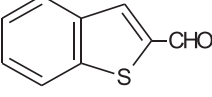
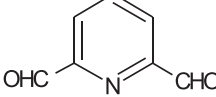
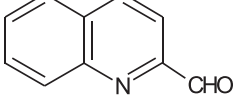
O and N Functionalization: Bandgap can also be engineered by O and N functionalization.^[78,79] Li et al.^[80] synthesized carbon nitride using urea by adding acrylamide, which leads to the addition of O and N components. The functionalization results in a lower bandgap energy of 2.24 eV compared to 2.48 eV for pure carbon nitride. The functionalized carbon nitride exhibited a six times higher photocatalytic hydrogen generation rate. Electron spin resonance (ESR) technique indicated that the narrowed bandgap is due to the increased electronic delocalization or lone-pair electron density with O and N functionalization. The different precursors for synthesizing carbon nitride could be used for bandgap engineering. Ragupathi et al. employed thiourea, urea and urea/glycine as the precursors.^[81] The values of bandgap energy of the fabricated carbon nitrides are 2.89, 2.78, and 2.35 eV, respectively. The significant reduction of the bandgap for urea/glycine samples drastically enhanced light harvest and photocatalytic performance.

Defects Engineering: One typical example of defects' effect on the photocatalytic HER is shown in Figure 3e. The absorption

band of defects-rich amorphous carbon nitride (DACN)-100 is red-shifted with a strong band tail compared with g-C₃N₄ (GCN), and the photocatalytic HER rate is dramatically increased by more than 8.6 times. Although the specific surface area is improved by 5.3 times caused by the reduced grain size of precursors, the enhanced visible light absorption caused by nitrogen-vacancy is still considered the main contributor to the better photocatalytic activity (Figure 3f).^[66,76,82,83] The calcination environment can also influence the formation of nitrogen-vacancy. Typically, carbon nitride samples are calcined in nitrogen, air, or carbon dioxide atmosphere, and the nitrogen-vacancy formation can be regulated.^[84] Therefore, control of defects in carbon nitrides is an effective strategy for enhancing photocatalytic activity.^[85–87]

Bandgap engineering has been one of the most valuable strategies for enhancing photocatalytic activity. Lowering the bandgap energy can expand the light absorption range, improve the carrier kinetic energy, and promote the hydrogen generation rate. However, too narrow bandgap generally leads to the CB negative than hydrogen electrode potential, resulting in the inhibition of

Table 1. Representative aromatics that can be grafted into carbon nitride networks and their corresponding precursors. Reproduced with permission.^[71] Copyright 2015, Elsevier.

Representative aromatics				
Corresponding precursors				
HER (μmol h ⁻¹)	226	218	255	236
Representative aromatics				
Corresponding precursors				
HER (μmol h ⁻¹)	270	332	280	130
Representative aromatics				
Corresponding precursors				
HER (μmol h ⁻¹)	323	358	343	294

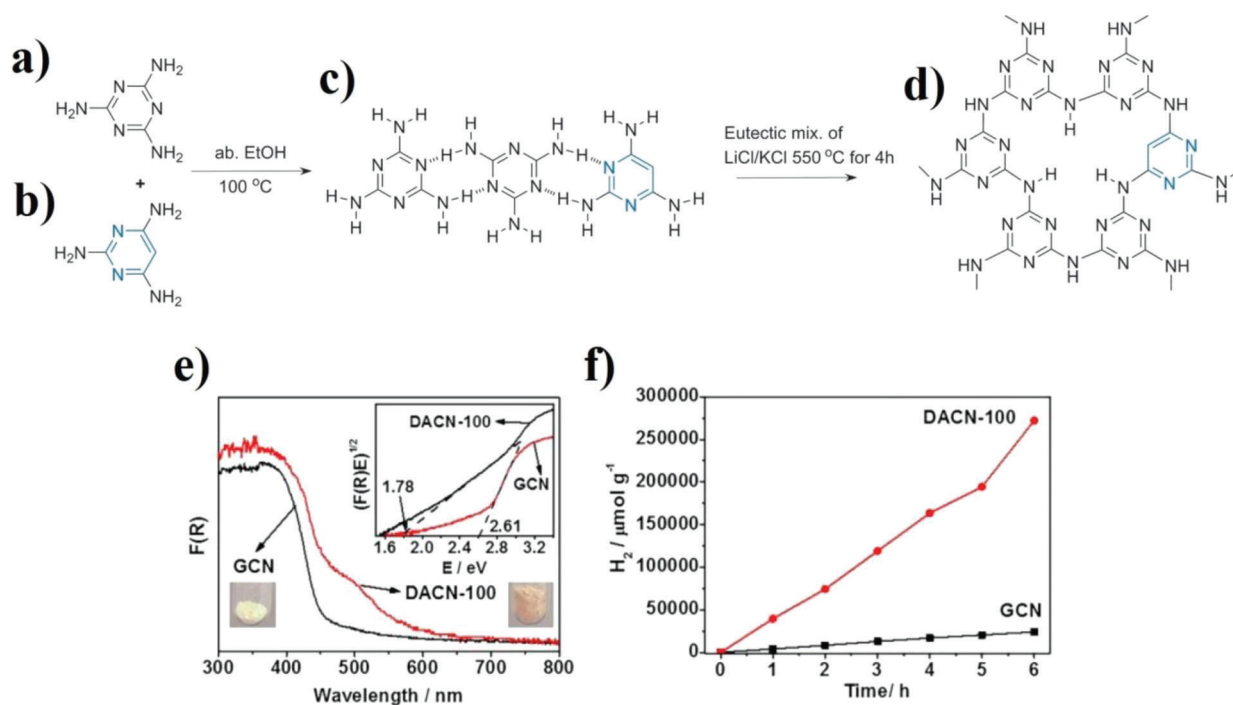


Figure 3. Scheme for the formation of the polytriazine imide samples. a) Melamine, b) 2,4,6-triaminopyrimidine, c) supramolecular aggregation, and d) the final proposed polytriazine imide structure. Reproduced with permission.^[75] Copyright 2014, Wiley-VCH. e) UV-vis diffuse reflectance spectra (inset: bandgap energies and photographs) and f) photocatalytic activities of graphite carbon nitride (GCN) and defect-rich amorphous CN (DACN-100) under irradiation with visible light. Reproduced with permission.^[76] Copyright 2018, American Chemical Society.

hydrogen production. A suitable bandgap is necessary for enhancing the photocatalytic efficiency.

3.1.2. Metal and Nonmetal Elements Doping: Different Excitation Mechanisms

Other than tuning carbon nitrides $\pi-\pi^*$ transitions, to produce a strong absorption peak at low wavelength,^[88] forming metal-to-ligand charge transfer (MLCT), is a practical way to extend the absorption band to lower energy regions (Figure 4a).^[89] By adding metal sources into the precursor of carbon nitrides, metal atoms can fill aromatic pores and coordinate with N atoms to allow new electronic states to emerge. With Pt as an example, in a Pt-LCT-participated photocatalytic system, C_3N_4 rings behave as hydrogen evolution sites, and charges are transferred from Pt atoms to C_3N_4 . This feature is validated by illuminating 420 and 550 nm monochromatic lights to samples with different Pt^{2+} concentrations. The comparable rates of all samples with different Pt^{2+} concentrations at 420 and 550 nm suggest that hydrogen evolution occurs on C_3N_4 rather than on Pt. The absorption band can be extended to 900 nm by incorporating a trace amount of Pt^{2+} , dramatically enhancing solar light's utilization (Figure 4b–d).^[89] The same work also confirms that non-noble metal elements, such as Cu, can achieve an enlarged absorption range and enhanced hydrogen production performance. MLCT can be formed on the C_3N_4 surface by incorporating metal sources after polymerization. In the case of Mn-modified C_3N_4 for oxygen evolution reaction (OER), electrons

are transferred from Mn atoms to C_3N_4 . Then, the Mn atoms can build MLCT to extend the absorption band and provide additional OER active sites. The sample with an optimized Mn content can reach production rates of $695.1 \mu\text{mol g}^{-1} \text{h}^{-1}$ for hydrogen and $332.4 \mu\text{mol g}^{-1} \text{h}^{-1}$ for oxygen in pure water in the presence of Pt as the cocatalyst.^[90] It is noted that the MLCT and the spin state of Mn strongly influence the hydrogen production performance.

The density functional theory (DFT) calculations showed that introducing transition metal atoms (e.g., Fe, Co, Ni, Cu, and Zn) could reduce the bandgap of $g-C_3N_4$, enhance the light absorption ability. The bandgap of metal-doped $g-C_3N_4$ can be tuned from 1.56 to 0.53 eV.^[91] The experimental results showed that nickel-doped carbon nitride obtained the highest hydrogen evolution rate ($354.9 \mu\text{mol h}^{-1} \text{g}^{-1}$) than those doped by Fe, Co, or Cu. Moreover, the performance is highly related to the oxidation state of single nickel atom sites and reaches the maximum at the Ni^{2+}/Ni^0 ratio of two. It should be noted that the performance would deteriorate dramatically if the ratio is not precisely at two. On the other hand, the highest photocatalytic hydrogen evolution rate of Cu-doped carbon nitride ($278.8 \mu\text{mol h}^{-1} \text{g}^{-1}$) is 21% lower than that of Ni doping, while the Cu-doped carbon nitrides experience less influence from the transition of the oxidation states of single copper atom.^[92]

Different from the coordination of metal-doped carbon nitrides, nonmetal elements are more likely to be a replacement in the framework. Zhang et al. used a hydrothermal method to obtain O-doped carbon nitride. Detailed characterization

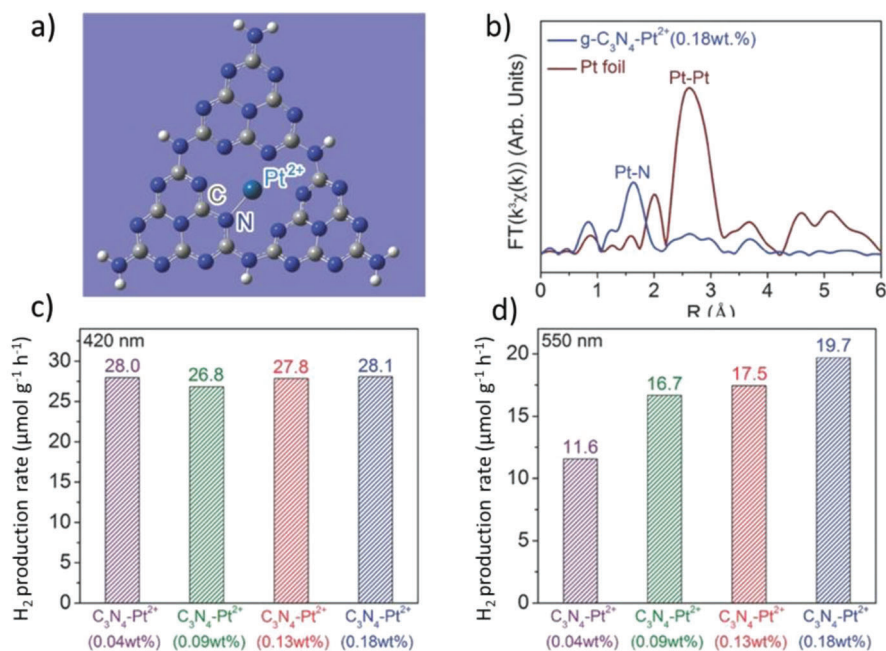


Figure 4. a) Structural illustration of the coordination of g-C₃N₄ with metal atoms, and b) k³-weighted Fourier-transform Pt L3-edge EXAFS spectra of Pt in g-C₃N₄ and hydrogen production rate under the illumination of c) 420 nm, and d) 550 nm. Reproduced with permission.^[89] Copyright 2016, Wiley-VCH.

indicated the oxygen atom replaced a nitrogen site in the structure. The oxygen-doped carbon nitride presented enhanced photocatalytic activity, with the hydrogen evolution rate increased by 11.3 times. Remarkably, since the crystal lattice distortion and the electronic polarization effect after introducing O element, an internal electric field would be constructed for enhancing the separation of electrons. Finally, the light harvest ability of the sample was enhanced across the whole wavelength range, and the bandgap was reduced by 0.11 eV.^[93] Another example of nonmetallic element doping is S-doped carbon nitride nanosheets. The significantly enhanced HER rate is due to the introduction of N defects and O functional groups by narrowing the bandgap, improving light absorption, and introducing active sites.^[94,95]

Table 2 summarizes metallic and nonmetallic doping of carbon nitride on HER performance. Although it can be seen that metal doping, functional group attachment and nonmetallic element doping can strongly influence the performance of photocatalytic HER, it is hard to screen out the best element. Still, the previous works provide some conclusive clues so far: 1) dopants can significantly enhance the light absorption ability of catalysts; 2) precious metal-doped carbon nitrides do not always take advantage of the low cost and abundant transition metal-doped carbon nitrides in photocatalytic hydrogen evolution activity enhancement; 3) the result exhibits no distinctive difference in the activity enhancement between metal doped and nonmetal doped carbon nitrides; 4) metal-doped carbon nitrides may provide intrinsic HER active sites. Overall, cheap transition metals, such as Fe, Ni, and Cu, could be desired candidates as dopants in carbon nitrides for photocatalytic hydrogen evolution.

3.2. Charge Carrier Transportation

3.2.1. Heterostructure-Assisted Electron Transfer

Heterostructured semiconductors can have three junctional modes: type I, type II, and type III. The heterostructures with type I and type II bandgaps are preferable in carbon nitride-based hydrogen evolution experiments (**Figure 5**). In contrast, the type III bandgap (**Figure 5c**) is unpopular due to its inactive electron interaction between two sides. A heterojunction with type-II band alignment can facilitate the transfer of excited electrons and the spatial separation of electrons and holes to hinder electron-hole recombination. In a typical P-N junction (type II staggered gap), major carriers of both p-type and n-type semiconductors will diffuse into the other side and form a depletion region with a built-in electric field spontaneously. The model of the P-N junction is given in **Figure 5d**. To simplify the expression, the photocatalysts on the left- and right-hand sides were defined as PC1 and PC2, respectively. Photoexcited electrons in the CB of PC2 and photoexcited holes in the VB of PC1 will migrate to the other side, respectively. As the photoexcited electrons and holes are separated spatially, the carrier recombination can be suppressed, leading to a longer charge pair's life span and increasing the possibility of charge utilization in redox reactions.

Despite that, a non-typical "P-N junction" formed by an n-type carbon nitride with another n-type semiconductor can also show superior performance in photocatalytic hydrogen evolution. It is well known that metal oxides have been widely used for energy-related applications,^[20,111] and they have extensively used to form heterostructure with carbon nitride for various catalytic reactions. For example, metal oxides like TiO₂,

Table 2. Doping effect on the performance of HER.

Materials	Enhancement (times)	H ₂ evolution rate [$\mu\text{mol h}^{-1}$]	Quantum efficiency	Light source	Refs.
Metal and nonmetal doping					
Mn + g-C ₃ N ₄ 20 mg	11	14 (O ₂ evolution: 6.6)	4% at 420 nm	300 W Xe lamp AM 1.5G	[90]
Br + g-C ₃ N ₄ 50 mg	2.4	48 (Separate experiment – O ₂ evolution: 4)		300 W Xe lamp $\lambda > 420$ nm	[96]
Fe + g-C ₃ N ₄ (25 mg L ⁻¹)	51.9	16200 ($\mu\text{mol h}^{-1} \text{g}^{-1}$)	0.8% overall	White LED	[97]
S + g-C ₃ N ₄ 50 mg	45	311	10% at 420 nm	500 W Xe lamp $\lambda > 420$ nm	[98]
O + g-C ₃ N ₄ 50 mg	41	8.7		300 W Xe lamp $\lambda > 400$ nm	[43]
Se + g-C ₃ N ₄ 50 mg	40	207	19.4% at 405 nm	300 W Xe lamp $\lambda > 420$ nm	[72]
B+ g-C ₃ N ₄	60	275 $\mu\text{mol h}^{-1}$	12.5% at 420 nm	$\lambda > 420$ nm	[99]
Ni+ g-C ₃ N ₄ 25 mg	37	8.9		300 W Xe lamp	[92]
Cu + g-C ₃ N ₄ 20 mg	30	212	5% at 420 nm	300 W Xe lamp $\lambda > 420$ nm	[100]
Pt + g-C ₃ N ₄ 100 mg	15	60		300 W Xe lamp $\lambda > 400$ nm	[89]
O + g-C ₃ N ₄ 12.5 mg	11.3	98.4	10.3% at 420 nm	300 W Xe lamp $\lambda > 420$ nm	[93]
Zn + g-C ₃ N ₄ 200 mg	10.8	59.5	3.2% at 420 nm	300 W Xe lamp $\lambda > 420$ nm	[101]
Na + g-C ₃ N ₄ 50 mg	9.5	8.45		300 W Xe lamp $\lambda > 420$ nm	[102]
Mo-Co + g-C ₃ N ₄ 100 mg	8.6	69		300 W Xe lamp $\lambda > 400$ nm	[103]
Cu + g-C ₃ N ₄ 100 mg	6.6	580	7.6% at 550 nm	300 W Xe lamp $\lambda > 420$ nm	[104]
S + g-C ₃ N ₄ 15 mg	3	127.4	8.35% at 420 nm	140 W Xe lamp	[94]
O + g-C ₃ N ₄ 25 mg	3.0	16	4.78% at 450 nm	300 W Xe lamp $\lambda > 420$ nm	[44]
Co + g-C ₃ N ₄ 80 mg	2.5	161	12.75% at 420 nm	300 W Xe lamp $\lambda > 400$ nm	[105]
P + g-C ₃ N ₄ 12.5 mg	2.0	11	1.48% at 500 nm	300 W Xe lamp $\lambda > 420$ nm	[106]
Organic molecules doping and functional groups introduction					
Pyromellitic dianhydride + g-C ₃ N ₄ 200 mg	3.0	21 (Separate experiment – O ₂ evolution: 7.7)	0.3% at 420 nm (0.2%)	300 W Xe lamp $\lambda > 420$ nm	[74]
Urea + g-C ₃ N ₄ 20 mg	30	56	17.9% at 400 nm	300 W Xe lamp 2000 nm > $\lambda > 200$ nm	[107]
Cyano groups + g-C ₃ N ₄ 50 mg	21	15	0.72% at 420 nm	300 W Xe lamp $\lambda > 420$ nm	[68]
Cyano groups and cyanamide groups + g-C ₃ N ₄ 20 mg	18	76		300 W Xe lamp $\lambda > 420$ nm	[108]

(Continued)

Table 2. (Continued).

Materials	Enhancement (times)	H ₂ evolution rate [$\mu\text{mol h}^{-1}$]	Quantum efficiency	Light source	Refs.
Cyano groups + atomically thin g-C ₃ N ₄ 20 mg	14	76	1.75% at 420 nm	300 W Xe lamp $\lambda > 420$ nm	[67]
2,4,6-triaminopyrimidine + polytriazine imide 25 mg	14	204	7% at 420 nm	300 W Xe lamp $\lambda > 420$ nm	[75]
Benzene + g-C ₃ N ₄ 10 mg	12	123	16% at 420 nm	300 W Xe lamp $\lambda > 420$ nm	
Carboxyl groups + g-C ₃ N ₄ 100 mg	9.0	200		300 W Xe lamp $\lambda > 420$ nm	[69]
N vacancy g-C ₃ N ₄ 50 mg	8.6	1884	34.4% at 400 nm	300 W Xe lamp $\lambda > 400$ nm	[76]
O + N vacancy polytriazine imide (1 mg/ml)	6.8	4907 ($\mu\text{mol h}^{-1}\text{g}^{-1}$)	3.4% at 420 nm	300 W Xe lamp $\lambda > 420$ nm	[109]
Quinoline + g-C ₃ N ₄ 100 mg	3.9	436	4% at 420 nm	300 W Xe lamp $\lambda > 420$ nm	[70]
Melamine + g-C ₃ N ₄ 14 mg	2.5	78		300 W Xe lamp 2000 nm $> \lambda > 200$ nm	[110]
N vacancy g-C ₃ N ₄ 5 mg	2.4	2.1	2.2% at 420 nm	300 W Xe lamp $\lambda > 420$ nm	[84]

$\alpha\text{-Fe}_2\text{O}_3$, In_2O_3 , etc.^[8,112–114] were successfully utilized to form hybrids/heterostructures with g-C₃N₄. Both g-C₃N₄ and metal oxides are n-type semiconductors, whereas their heterojunction can still behave like a P–N junction because of the difference in electron affinity across the two sides.

In some cases, as illustrated in Figure 5e,f, the intrinsic Fermi level of the n-type semiconductor is higher than the intrinsic Fermi level of the p-type semiconductor. The direction of the built-in electric field is opposite to that of normal P–N junctions; thus, the direction of electron transfer is reversed. The excited electrons on the CB of PC1 will be transferred to the VB of PC2 to recombine with excited holes, resulting in spatially separated electrons and holes and a reduced recombination rate. A junction with such an electron transfer behavior is called a Z-scheme junction. Z-scheme junctions can be built by strategies, either direct contact or using a conductor as a mediator of two semiconductors (Figure 5f). In a Z-scheme heterostructure (Figure 5e), some photoexcited electrons from one part will be sacrificed by the other part, that is, the photogenerated electrons in PC1 recombine with photogenerated holes in PC2, and the active electrons in CB of PC2 and holes in VB of PC1 participate in the photocatalytic reaction. Figure 5e is the direct contact structure of PC1 and PC2, sometimes called S-scheme due to electric field-assisted electron/hole recombination.^[115–117] Figure 5f is composed of a conductor between PC1 and PC2, facilitating the recombination of electrons and holes in PC1 and PC2, respectively. In this situation, one may think that Z-scheme heterojunctions waste a large portion of energy on the designated electron–hole recombination. While separated charges in Z-scheme junctions do not lose energy caused by the band transition, the system can maintain its highest oxidation and reduction ability. Thus Z-scheme heterojunctions are comparable or even superior to normal P–N

junctions.^[118] However, this concept may not be correct in some conditions because the position of the conduction band of PC 2 in Figure 5e,f may also decline after the Fermi level equilibration.

The intrinsic property of the material determines the transfer behavior of electrons in the heterojunction, and then the junction will be either a normal P–N junction or a Z-scheme junction. Therefore, it may not be wise to argue the advantages or drawbacks by comparing a normal P–N junction and a Z-scheme junction. Optimizing both junctions is an effective strategy to achieve enhanced photocatalytic HER. More recently, an M-Scheme of CeO₂/Ti₃C₂/TiO₂ was proposed, in which, the excited electrons from CeO₂ and TiO₂ were transferred to Ti₃C₂ and the left holes in CeO₂ and TiO₂ take part in the oxidation process.^[119] These processes can reduce the charge transfer path and utilize excited electrons from both CeO₂ and TiO₂.

Under some conditions, the P–N and Z-scheme junction in different hole scavengers could be switched. A typical example was demonstrated in the W₁₈O₄₉/g-C₃N₄ heterojunction.^[120] In pure water or methanol/water solution, the Fermi level of W₁₈O₄₉ is higher than that of g-C₃N₄, and a normal P–N junction can be formed consequently (Figure 6a). By interacting with triethanolamine (TEOA), the Fermi level of g-C₃N₄ can be uplifted higher than that of W₁₈O₄₉, and the direction of the built-in electric field is reversed, making the P–N junction changed to a Z-scheme junction (Figure 6b). The interaction between g-C₃N₄ and TEOA revealed that TEOA is superior to methanol as an electron donor in the photocatalytic HER process.

A few techniques can be used to validate the Z-scheme mechanism in the heterojunction based on its unique behaviors. In the ideal case of a type II heterojunction (P–N junction), as shown in Figure 7a, photon-excited charges and holes will accumulate on PC1 and PC2, respectively. In this case, water reduction

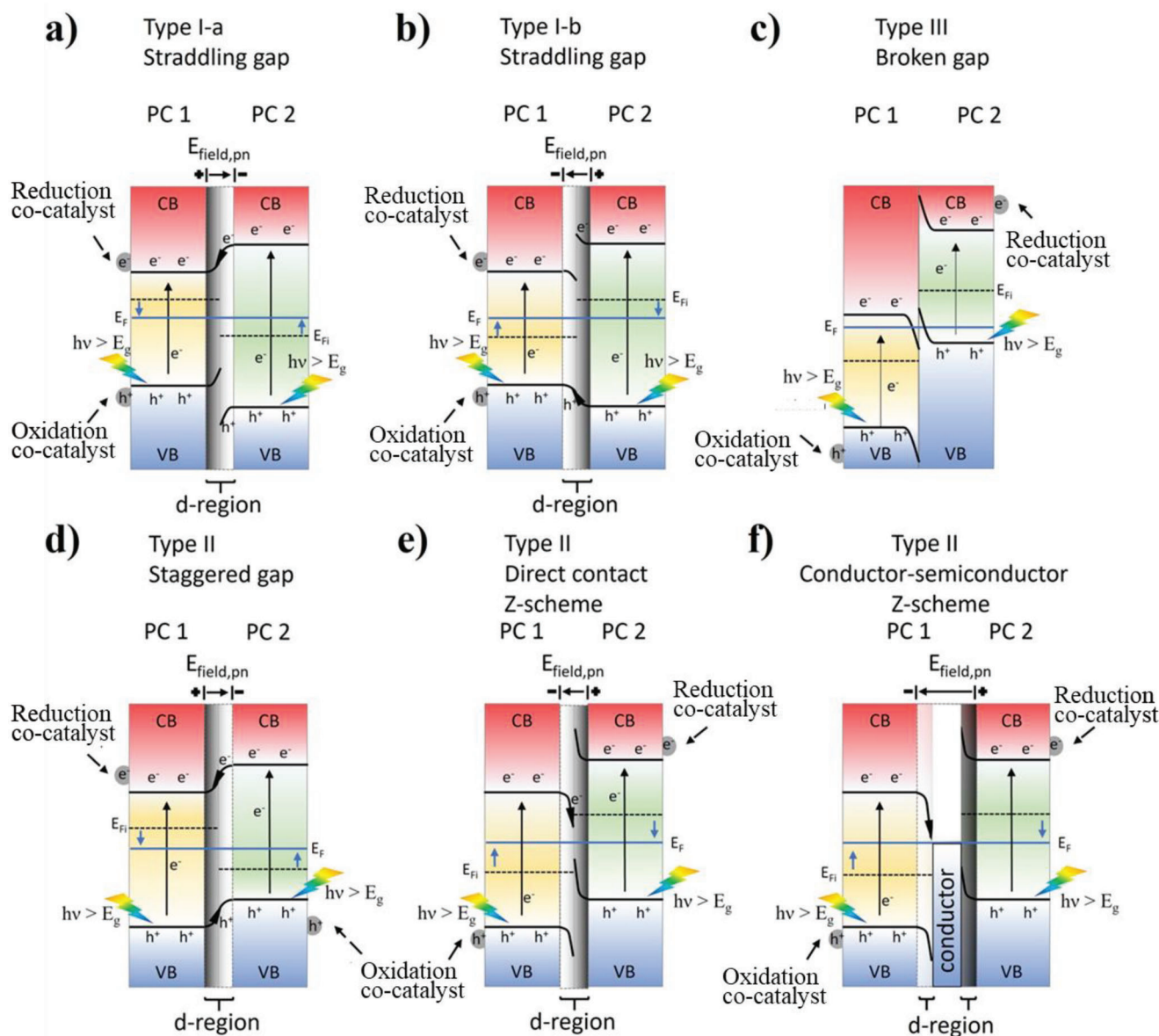


Figure 5. The band structure of a) type I-a and b) type I-b heterojunctions with a straddling gap, c) type III heterojunctions with a broken gap, d) type II heterojunctions with a staggered gap and e) and f) Z-scheme heterojunction as a particular case of type II heterojunction.

reactions occur on PC1, and water oxidation reactions occur on PC2. Hence $\cdot\text{O}_2^-$ and $\cdot\text{OH}$ radicals should not be present in final products. By employing the electron spin resonance (ESR) technique, the produced $\cdot\text{O}_2^-$ and $\cdot\text{OH}$ radicals can be simultaneously detected, which can be an evidence of forming a Z-scheme heterojunction.^[113,121] Trapping experiments can also be performed to identify active radicals by incorporating rhodamine B (RhB) with radical scavengers.^[122] However, the hypothesis may not be correct in practice because there may be only a part of photoexcited electrons in the CB of PC2 transferring to the CB of PC1, and reduction reactions may still occur at PC2, especially for the large grain size. Therefore, $\cdot\text{O}_2^-$ radicals can be produced while the Z-scheme junction is not fully formed. It's similar to photoexcited holes and $\cdot\text{OH}$ radicals. Like the proposed mecha-

nism in the CN/Mn-N-TiO₂ heterostructure, a part of the holes has been transferred from PC1 to PC2. As a consequence, extra photoexcited holes can still generate $\cdot\text{OH}$ radicals.^[123]

Time-resolved photoluminescence (TRPL) spectra can be used to analyze the charge carrier dynamics. The decay spectrum can be fitted to a triple exponential function^[124]:

$$I(t) = \sum_i^n A_i e^{-t/\tau_i} \quad (1)$$

where $I(t)$ is the intensity of the spectrum, τ_i is the photoluminescence (PL) lifetime, and A_i is the corresponding coefficients as normalized percentages. The mean PL lifetimes can be calculated as $\tau_m = \frac{\sum_{i=1}^n A_i \tau_i^2}{\sum_{i=1}^n A_i \tau_i}$. The nonradiative recombination of

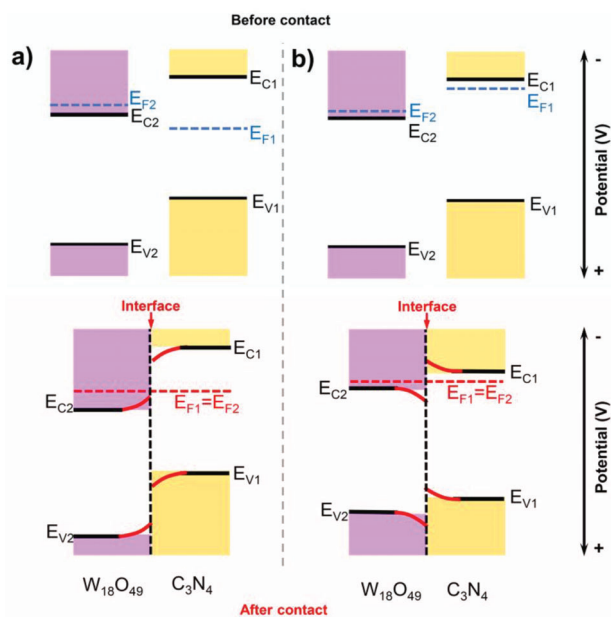


Figure 6. Schematic energy band diagrams of $W_{18}O_{49}$ and C_3N_4 in a) pure water and b) triethanolamine (TEOA) solution. Reproduced with permission.^[120] Copyright 2017, Elsevier.

surface-trapped electron and hole pairs contributes to the value of τ_1 and τ_2 as short lifetime components, and τ_3 represents the recombination of free excited electrons as the extended lifetime component. As shown in Figure 7b, photoexcited electrons in the CB of PC1 will recombine with photoexcited holes in the VB of PC2 before the natural recombination. Therefore, at least an accelerated PL decay in long-lifetime components should be observed if a Z-scheme junction is constructed and, typically, short-lifetime components are also accelerated.^[114,125–128] In some exceptional cases, extended lifetime is still used as evidence of Z-scheme heterojunction, and the reason is unclear.^[129]

Although type II heterostructure is usually preferred in photocatalyst engineering, some type I heterostructures can also provide excellent photocatalytic performance. In the amino-modified $ZnIn_2S_4$ (AZIS) nanoflower with benzoic acid functionalized carbon nitride, both photoexcited electrons and holes from the carbon nitride part are going to migrate to the $ZnIn_2S_4$ domain (Figure 8).^[130] The proposed enhancement mechanism as a condensed connection between AZIS and BCN may not be convincing because the driving force of both electrons and holes is reduced.^[130] One possible mechanism could be the built-in electric field facilitating electrons or holes transferring, and part of electron–hole pairs are separated spatially, thus increasing the lifespan of charge carriers. The effect of charge separation overcomes the impact of reduced redox ability, and then the type I heterostructure eventually benefits the photocatalytic activity.

A PN junction can also be built at the molecular level. As mentioned in Section 3.1.1, doping with quinoline molecules changed the excitation mechanism and reduced the bandgap. Differently, in the case of selenium doped and cyanamide functionalized carbon nitride, as illustrated in Figure 9b, doped selenium and functional groups can change the regional electron affinity, thus forming an ambipolar conjugated semiconductor. The sample con-

taining both n-type and p-type conductivities is justified by showing both positive and negative slopes in the Mott-Schottky measurement (Figure 9a).^[72] These binary junctions can also be considered ternary junctions, and the undoped heptazine units behave as a mediator between the electron donor and acceptor.^[108]

Although the formation of heterojunction can facilitate the electron transport and suppress the electron–hole recombination, the quantum yield (QY) providing the intrinsic property of the photocatalytic system is challenging to measure, and the enhancement can be overestimated due to the nonlinearity of light absorption in respect of the concentration of each photocatalyst. According to the estimation, the enhancement could be up to 31% in the case of a standard Pt-TiO₂-g-C₃N₄ model. The experiment is better performed in the linearizable regime to minimize the artificial enhancement. Mass normalization should be avoided if photocatalysts have a significant contrast of the absorption cross-section of two photocatalysts and the larger absorbance photocatalyst usually has a smaller bandgap due to the more extensive absorption range.^[131]

Table 3 summarizes different types of heterostructures and their performance in photocatalytic HER. Both P–N and Z-scheme junction-engineered photocatalysts are efficient for photocatalytic hydrogen evolution activity according to the table. The enhanced photocatalytic activity is primarily ascribed to the spatial separation and the prolonged life span of charge carriers. Nevertheless, two different charge carrier migration strategies do not show distinct advantages over each other based on the summarized results. The electronic property of the catalysts determines the electron transfer mode, and then the conversion between PN junctions and Z-scheme heterostructures is barely possible. A possible way to convert a PN junction to a Z-scheme heterostructure is to introduce an electron mediator between two catalysts (Figure 5f) like TiO₂/g-C₃N₄^[132,133] and NiFe₂O₄/g-C₃N₄. The NiFe₂O₄/g-C₃N₄ binary catalyst is a PN junction, and the NiFe₂O₄/carbon dots/g-C₃N₄ ternary catalyst is turned into a Z-scheme heterostructure by the intercalated carbon dots. It turned out that the ternary composite's organic pollutant degradation ability was doubled compared to the binary composite. However, in photocatalytic hydrogen evolution, the TiO₂/benzoic acid/g-C₃N₄ Z-scheme heterostructure has no advantage over the binary catalyst without the electron mediator, and the enhancement factor of the ternary catalyst is less than one-sixth of the binary catalyst. The conversion of electron transfer modes by inserting electron mediators is not proven in other research articles since there are plenty of examples that PN junctions engineered with built-in electron mediators.^[8,134] Therefore, the electron transfer mode should have less priority at the experiment design stage. Considering the hydrogen evolution performance with the element abundance and low toxicity, TiO₂ and Fe₂O₃ are well studied and could be two suitable candidates for heterostructure engineering with carbon nitride despite the electron transfer mode.

3.2.2. Crystallinity and Crystal Phases Orientation: Electron Migration Preference

Carbon nitrides in an ordered crystal structure have a better charge transfer ability than those of a disordered or amorphous

Table 3. Summary of different types of heterostructures, their testing parameters, and HER performance.

Heterostructures	Enhancement (times)	H ₂ evolution rate [$\mu\text{mol h}^{-1}$]	Quantum efficiency	Light source	Refs.
C _{ring} /C ₃ N ₄ 30 mg	10	11.1 (O ₂ evolution: 5.5)	5% at 420 nm	300 W Xe lamp AM 1.5G	[135]
Carbon nanotube + Co/g-C ₃ N ₄ 20 mg	172	24.16		150 W Xe lamp $\lambda > 400$ nm	[136]
Ni @ C/g-C ₃ N ₄ 30 mg	88	64.5	2.14% at 420 nm	300 W Xe lamp $\lambda > 420$ nm	[137]
Ag @ C ₃ N ₄ 25 mg	30	25.2		300 W Xe lamp $\lambda > 420$ nm	[138]
Carbon nanofibers /g-C ₃ N ₄ 10 mg	9.9	460	14.3% at 420 nm	300 W Xe lamp $\lambda > 420$ nm	[139]
Graphitized carbon/g-C ₃ N ₄ 100 mg	5	79.3		300 W Xe lamp $\lambda > 400$ nm	[140]
Black phosphorus /g-C ₃ N ₄ 100 mg	3.6	90		300 W Xe lamp $\lambda > 420$ nm	[141]
Carbon nanotube / g-C ₃ N ₄ 60 mg	3.4	10		150 W Xe lamp $\lambda > 400$ nm	[142]
AgBr/g-C ₃ N ₄ 100 mg	13	369	5.51% at 420 nm	300 W Xe lamp $\lambda > 420$ nm	[126]
TiO ₂ /g-C ₃ N ₄ 100 mg	10.8	51.3	0.31% at 420 nm	300 W Xe lamp $\lambda > 420$ nm	[132]
Meso-tetrakis-(meta-carboxyphenyl)- porphyrin / g-C ₃ N ₄ 15 mg	8.36	54		Mercury vapor lamp	[143]
TiO ₂ /Au/g-C ₃ N ₄ 250 mg	6	87.5	0.588% Full spectrum	150 W Ceramic metal-halide lamp	[8]
In ₂ O ₃ /g-C ₃ N ₄ 5 mg	5	5		300 W Xe lamp $\lambda > 420$ nm	[114]
SrTa ₂ O ₆ /g-C ₃ N ₄ 50 mg	4.77	37.2	2.62% at 420 nm	300 W Xe lamp $\lambda > 420$ nm	[144]
WS ₂ /Ag/g-C ₃ N ₄ 100 mg	2.5	68.62		300 W Xe lamp	[134]
Mn-N-TiO ₂ /g-C ₃ N ₄ 45 mg		39.15		300 W Xe lamp	[123]
C ₃ N ₄ /NiO/NiS _x	347	1248.1 g ⁻¹ $\mu\text{mol h}^{-1}$	NA	300 W Xenon lamp 420 nm	[145]
MoN/g-C ₃ N ₄	120	240 g ⁻¹ $\mu\text{mol h}^{-1}$	0.09%	Xe lamp (300 W)	[146]
g-C ₃ N ₄ -PANI Z-scheme	16	3164.3 g ⁻¹ $\mu\text{mol h}^{-1}$	NA	300 W Xenon lamp 420 nm	[147]
Perylene diimide polymer/rGO/g-C ₃ N ₄ 25 mg	12.1	15.8 (O ₂ evolution: 7.8)	4.94% at 420 nm	300 W Xe lamp $\lambda > 420$ nm	[125]
α -Fe ₂ O ₃ /g-C ₃ N ₄ 10 mg	9.8	314 (separate experiment – O ₂ evolution: 19.1)	44.35% at 420 nm	300 W Xe lamp $\lambda > 420$ nm	[113]
NiCo ₂ O ₄ /g-C ₃ N ₄ 20 mg	83	109.6	4.5% at 400 nm	300 W Xe lamp $\lambda > 400$ nm	[122]
MnIn ₂ S ₄ /g-C ₃ N ₄ 50 mg	8.2	10		300 W Xe lamp $\lambda > 400$ nm	[121]
WO ₃ /g-C ₃ N ₄ 50 mg	7	156		300 W Xe lamp	[128]
H ₃ PW ₁₂ O ₄₀ /g-C ₃ N ₄ 5 mg	2.2	14.6		300 W Xe lamp AM 1.5G	[129]
TiO ₂ /Benzoic acid /g-C ₃ N ₄ 20 mg	1.6	22.46		300 W Xe lamp $\lambda > 420$ nm	[133]
W ₁₈ O ₄₉ /g-C ₃ N ₄ 50 mg	1.57	51	39.1% at 420 nm	300 W Xe lamp $\lambda > 420$ nm	[120]

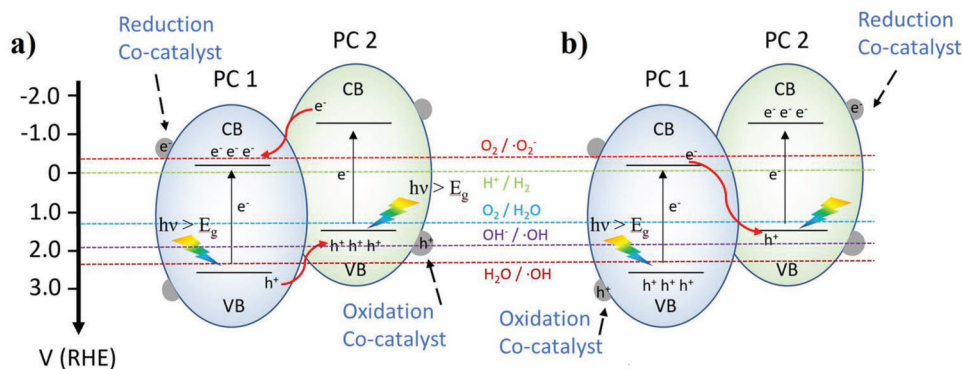


Figure 7. Products of water splitting at different potentials. a) Type II heterojunction; b) Z-scheme heterostructure.

form because the layer stacking distance of carbon nitrides dominates charge mobility and an ordered structure has a reduced stacking distance. A better crystalline structure can benefit charge transfer and thus photocatalytic HER rate.^[148] However, better charge transferability results in faster electron–hole recombination, and better crystallinity normally causes an increased intrinsic bandgap.^[149] Both are unfavorable to a high photocatalytic HER performance and so the crystallinity should be carefully optimized for achieving maximum photoactivity.

Since electrons have a preferred direction during migration in the crystal lattice, the crystal phase exposed to the reaction solution is an essential factor in photocatalysis. In the case of highly crystallized triazine-based carbon nitride, it has been proved that the prismatic (101–0) plane is more active in hydrogen evolution compared with the basal (0001) plane (Figure 10a,b). According to theoretical calculations, the charge density preferred to accumulate on the conjugated layers ((0001) plane) over the interlayer, confirming the realization of electron-directed transfer through the crystal phase regulation strategy. Since the higher electron availability, Pt or other cocatalysts are expected to be deposited on (101–0) facets (Figure 10c), which enhances the charge transfer

kinetics. In photocatalysis for water splitting, the catalytic activity is gradually promoted with the increase of the ratio of (10 $\bar{1}$ 0) and (0001) planes, where the maximum O₂ and H₂ evolution rates of 91 and 189 $\mu\text{mol h}^{-1}$ at a ratio of 4.70.^[77]

Inspired by the extension of the conjugated network and the participation of lone pair on the N atom with the π conjugated system of heptazine motif, C_xN_y with different C/N ratios, such as C₃N₅, C₃N₃, C₄N₃, C₃N, and C₂N were designed and developed recently.^[150–155] In the case of 3-amino-1,2,4-triazole derived C₃N₅, the new-structured C₃N₅ with conjugated heterocyclic ring possessed a narrower bandgap (2.2 eV), leading to the improvement of π – π^* (400–550 nm) and n – π^* (250 nm) electronic transition.^[156] Analogously, using the thermal deammoniation strategy, 2,5,8-trihydrazino-s-heptazine was converted into C₃N₅ containing heptazine moieties bridged together by azo linkage. Noteworthy, due to the overlapping of p orbitals on the N atoms in azo bond and π system, the π conjugated network of the heptazine motif is expanded by the incorporation of the azo linkage, leading to the reduction of bandgap (1.76 eV).^[157] Developing a lower C/N ratio of carbon nitride is another alternative strategy for increasing the delocalization of π -electrons. For instance, a well-defined C₅N₂ with a conjugated C=N linkage was obtained, which broke the limitation of electrons delocalization in HOMO/LUMO orbitals caused by tertiary N linkage in g-C₃N₄, thereby strengthening the delocalization of π -electrons in C₅N₂.^[150]

Generally, g-C₃N₄ shows an amorphous crystal structure, and the crystallinity is hard to be improved with typical thermal condensation methods, especially in the form of an in-plane (100) phase. The salt confinement/molten method is the most efficient way to obtain a highly ordered in-plane structure. Alkali metal ions (Na⁺ & K⁺) rearranged the in-plane and out-plane structures of g-C₃N₄, resulting in the structural transformation from amorphous to a crystalline structure. The highly crystallized g-C₃N₄ has advantages in separating electrons and holes ascribed to the lower impedance.^[158,159]

3.2.3. Charge Transportation Channels: Efficient Electron–Hole Pair Migration

Achieving efficient charge transfer in carbon nitrides could be a prerequisite for performing highly efficient solar energy harvest.

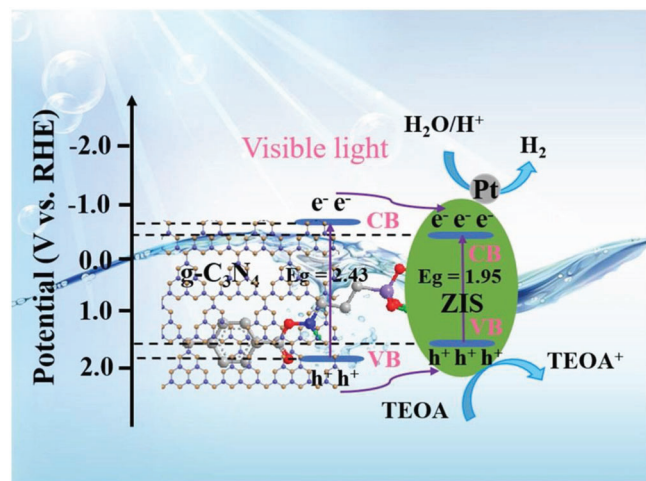


Figure 8. Photocatalytic mechanism of the charge transfer for hydrogen generation over the BCN/AZIS under visible light irradiation. Reproduced with permission.^[130] Copyright 2019, Elsevier.

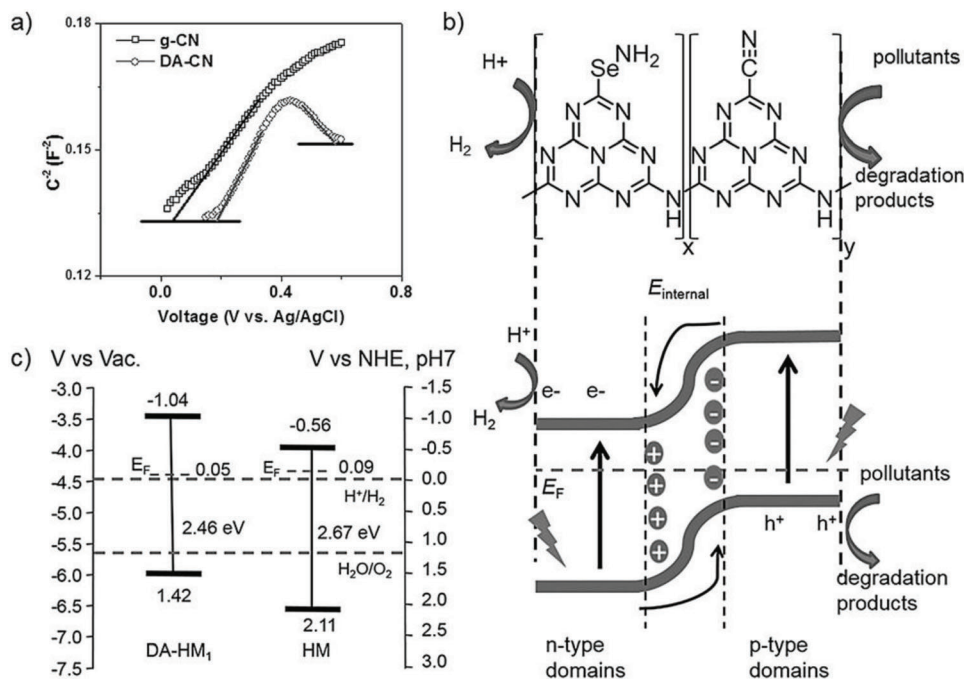


Figure 9. a) Mott-Schottky plots for heptazine-based melon (HM) and donor-acceptor-HM (DA-HM1). b) Illustration of charge transfer in the p-n homojunction of DA-HM and c) schematic energy-level diagrams of HM and DA-HM1. Reproduced with permission.^[72] Copyright 2018, Wiley-VCH.

Other than establishing a heterostructure to promote directional charge transfer, which can be engineered easily, the intrinsic charge transfer in a single photocatalyst is undirected and hard to be controlled. Unlike forming an MLCT, doped Cu atoms in carbon nitrides can bond with N atoms and create highly efficient charge transfer channels (Figure 11a,b). As a different preparation method, Cu atoms are prelocalized within the layers of the precursor before pyrolysis. After the synthesis, Cu-incorporated carbon nitride does not show a strong extended absorption band, which indicates MLCT is not the dominant mechanism. However, the lifespan of electron-hole pairs and the impedance are reduced, which means better charge transferability. The theoretical calculations showed that Cu atoms were either bonded with three in-plane N atoms or four N atoms across two neighboring lay-

ers, which improved intralayer and interlayer charge transfer.^[100] Although the MLCT could not be the dominant mechanism in some metal-doped carbon nitride samples, the density functional theory (DFT) calculations indicated the metal-doped samples could have a stronger absorption ability than only having electron transportation tunnels. The bandgap of pristine carbon nitride could decrease from 2.135 eV to 1.44 eV and 1.5 eV with Co and Mo dopants, respectively. From the experimental results, the absorption edge is only red-shifted by 5 nm.^[103] The inconsistency between theoretical calculations and experimental results could be ascribed to the low doping concentration or the heterogeneous distribution between the surface and the inner part. Both possibilities strongly influence the intrinsic band-to-band absorption of carbon nitrides. At higher Mo concentrations in carbon nitride,

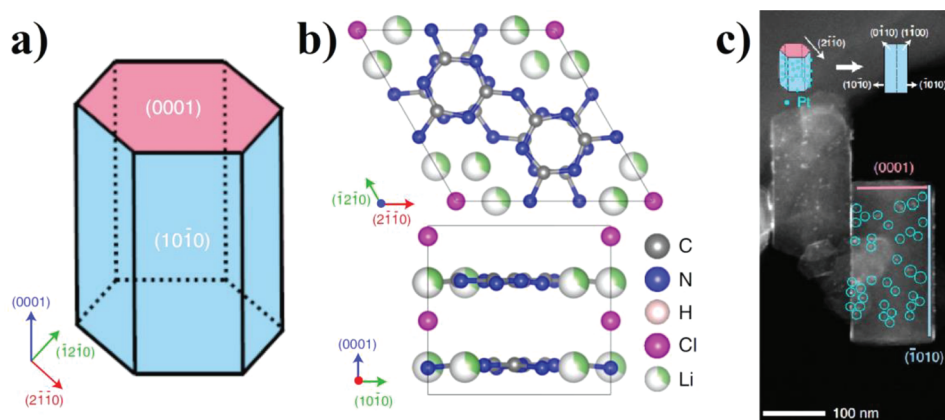


Figure 10. a) Schematic illustration of the triazine-based carbon nitride (polytriazine imides, PTI)/Li⁺Cl⁻ crystal, b) the crystal structure of PTI/Li⁺Cl⁻, and c) the HAADF-STEM image of a PTI crystal aligned to the (2110) direction. Reproduced with permission.^[77] Copyright 2020, Springer Nature.

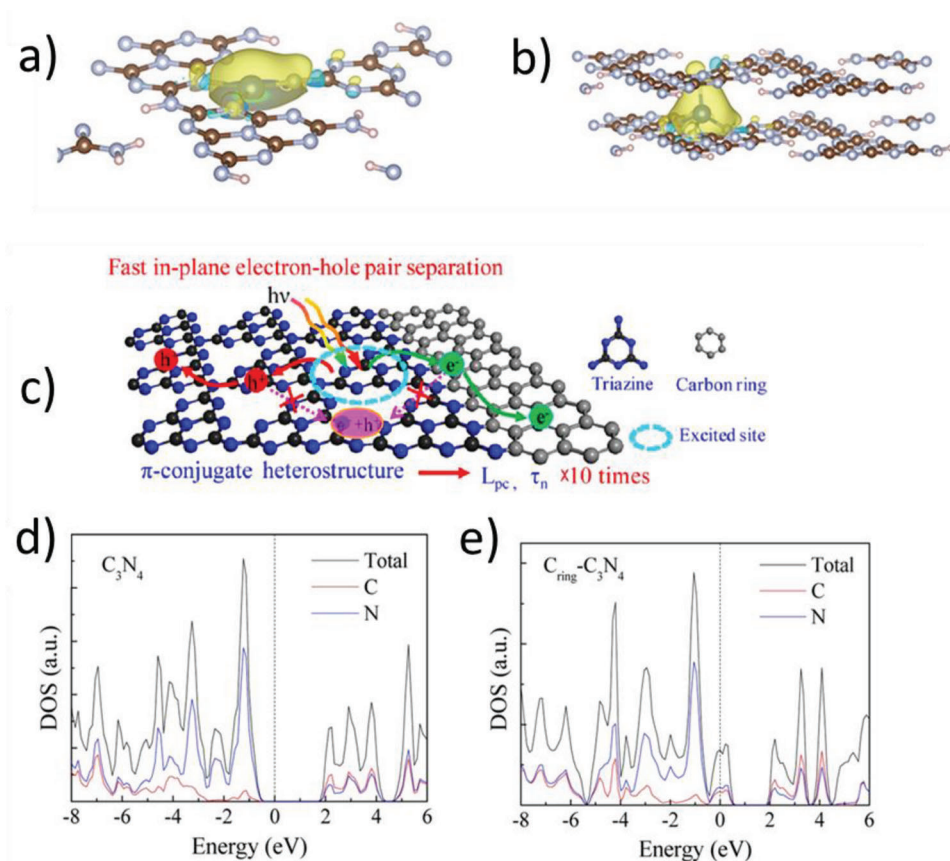


Figure 11. Calculated charge difference surfaces of the a) Cu-N3 and b) Cu-N4 coordination systems. Reproduced with permission.^[100] Copyright 2020, Wiley-VCH. Schematic for c) photocarrier transfer in $(C_{ring})-C_3N_4$, where L_{pc} and τ_n represent the photocarrier diffusion length and lifetime, respectively. d) Calculated DOSs for pristine $g-C_3N_4$ and e) $(C_{ring})-C_3N_4$. Reproduced with permission.^[135] Copyright 2017, American Chemical Society.

the color of samples may turn black, and the properties of the materials will vary significantly.^[160] Therefore, optimizing doping concentration and uniform distribution of dopants are essential for achieving high-performance photocatalytic activity.

Different from building a heterojunction with a semiconductor, carbon nitrides incorporated with carbon compounds can facilitate the photoexcited electron transfer benefiting from the high conductivity of graphite/graphene (Figure 11c).^[135,161] By connecting these two different electron affinity catalysts, an in-plane π -conjugated heterostructure is designed ($(C_{ring})-C_3N_4$). Both experimental results and theoretical calculations revealed that an intermediate state located at ≈ 0.5 eV above the valence band was formed. Moreover, the bandgap of $(C_{ring})-C_3N_4$ reduced 0.2 eV in comparison of $g-C_3N_4$. Leveraging above two advantages, it is possible to reduce the overpotential of reduction reaction. Notably, the surface N sites in $(C_{ring})-C_3N_4$ exhibited larger H_2O adsorption energy of 1.10 eV, which showed the H_2 evolution rates of $371 \mu\text{mol g}^{-1} \text{h}^{-1}$ with a quantum yield of 5% at 420 nm (Figure 11d,e).^[135] Carbon and carbon-related materials are commonly used to build heterostructures with carbon nitrides to improve the charge carrier transfer, thus benefiting photocatalytic HER activity.^[139,140,142,162]

However, the loading amount and physical properties of carbon materials can result in different photocatalytic perfor-

mances. Among single-walled, double-walled, and multiwalled carbon nanotubes, 0.5 wt% single-walled carbon nanotubes loading is the optimized case. The most efficient electron transfer is ascribed to the 1D pathway of single-walled nanotubes. Increasing the number of carbon nanotube walls can result in a 2D transport pathway and thus reduce electron transport efficiency. The photocatalytic performance of single-walled carbon nanotube/ $g-C_3N_4$ heterostructure is increased up to 3.4 times that of unmodified carbon nitride, while the ratio of optimized carbon ring/ $g-C_3N_4$ is 10.^[135,142] $g-C_3N_4$ with graphene or graphene oxide has also been widely investigated. Incorporating graphene or graphene oxide can increase the conductivity due to its excellent conductivity and act as the charge transfer channel, thus enhancing the HER performance.^[163–165]

Besides carbon, doping with other nonmetallic elements has also been extensively investigated. For example, Zhu et al. and Liu et al. discovered that a small P doping in $g-C_3N_4$ could significantly enhance the photocatalytic hydrogen generation rate. The resistance was strongly reduced, strengthening the carrier's transportation rate.^[166,167] In another work, P and S were doped into carbon nitride, and the photocatalytic activity increased over six times higher than undoped carbon nitride. The enhanced active sites and recombination suppression are major reasons for the enhancement. However, the reduced impedance also plays a

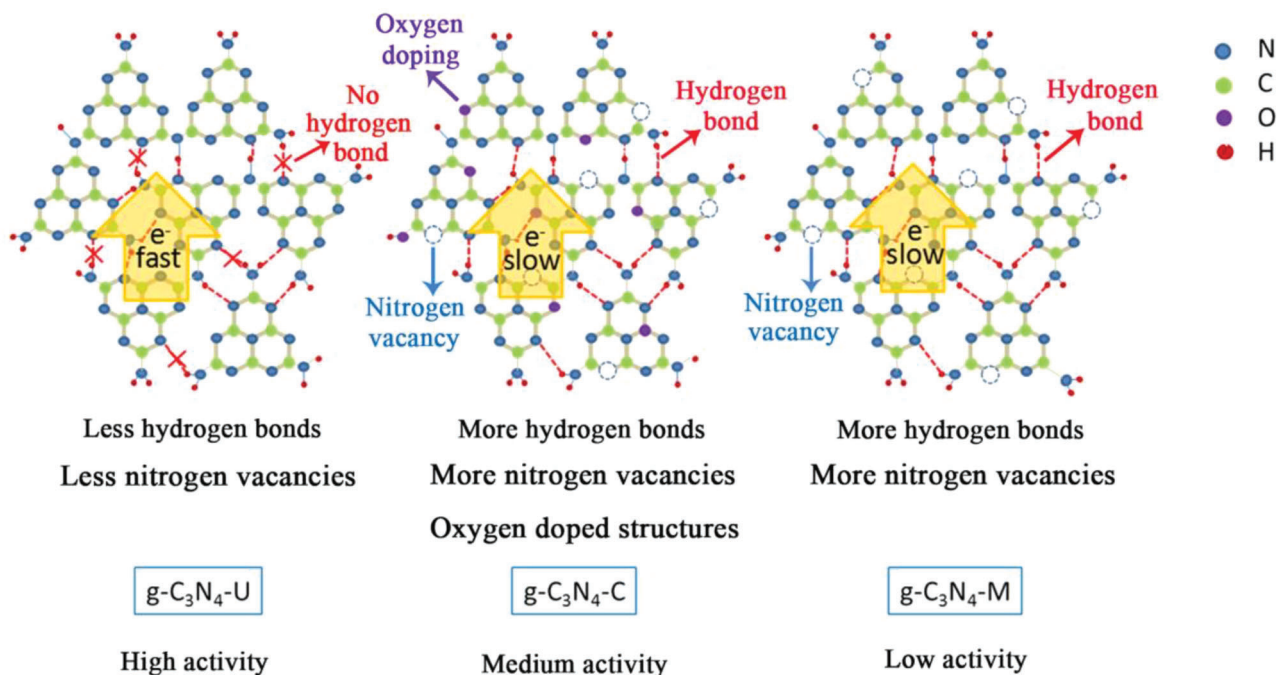


Figure 12. Schematic illustration of the mechanism for synergetic photocatalysis over $g\text{-C}_3\text{N}_4$ derived from different precursors. Reproduced with permission.^[82] Copyright 2016, Elsevier.

critical role.^[168] Interestingly, Liu et al. used a simple method to integrate chlorine into $g\text{-C}_3\text{N}_4$, which showed 19.2 times higher hydrogen evolution rate than pure $g\text{-C}_3\text{N}_4$ and achieved 11.2% AQY at 420 nm, which is very high compared to other reports. Though different parameters can influence the performance, reducing the bandgap by chlorine doping is one of the determining factors which leads to lowering the impedance. Therefore, non-metallic doping should be paid attention to for enhancing the photocatalytic performance of $g\text{-C}_3\text{N}_4$.^[169] It is to note for this low-cost nonmetallic element doping, the stability should be carefully considered since chlorine may be easily leached out during photocatalysis.

In the above discussion, we have introduced several strategies to enhance charge transfer, such as bandgap engineering, which reduces the bandgap and improves the conductivity for overall charge transfer. Metallic and nonmetallic doping can significantly increase the conductivity of the materials, though increased active sites and suppression of recombination of electron/holes also apparently contribute to enhanced photocatalytic activity. On the other hand, as discussed previously, the heterostructure can form a built-in electric field, which strongly suppresses the recombination, whereas the electric field also provides a directional charge transport channel with high kinetics.

3.2.4. Polymerization: Adverse Effect of Hydrogen Bond

Different precursors of carbon nitride can result in a difference in the degree of polymerization. As discussed previously, most of the synthesized carbon nitride is in the amorphous state, significantly influencing its HER performance. Molten salt method has been employed to improve the degree of poly-

merization and crystallinity. On the other hand, the degree of polymerization of carbon nitride can determine the number of hydrogen bonds, whereas, it was found that the existence of hydrogen bonds could reduce the electron transfer efficiency, thus reducing the photocatalytic HER rate.^[82] For example, compared with carbon nitride prepared with melamine and cyanamide, the sample from urea has fewer hydrogen bonds which can be proved by XRD and FTIR, resulting in a higher hydrogen evolution rate (Figure 12).^[82] People may argue that fewer hydrogen bonds may be accompanied with nitrogen vacancy and other factors. Lan et al. investigated hydrogen bond and nitrogen vacancies contribute to HER. It was discovered that fewer hydrogen bonds and nitrogen vacancies exhibited the highest activity, though late experiment showed that oxygen addition could influence the activity, whereas hydrogen bonds play the dominant role (Figure 12).^[82,170] Besides the precursors effect on polymerization, post-thermal treatment can break hydrogen bonds and improve the photocatalytic activity of the treated sample.^[171] The loss of hydrogen bond can lead to the increase in band tails or localized states near the band edges, which can increase in optical light adsorption and lower the bandgap, thus increase the charge transfer kinetics. Notably, thermal treatment may increase the number of nitrogen vacancies and pores in carbon nitride due to the loss of hydrogen bond, which may also contribute to the HER enhancement.

Though breaking hydrogen bonds is considered as an effective way for enhancing HER performance, people also argued that nitrogen vacancies strongly enhanced HER performance. For example, Liu et al. developed a different method after the polymerization of the precursor by treating the pristine carbon nitride using hydrogen to create nitrogen vacancies that enhanced

the hydrogen evolution three times higher.^[172] Likewise, using 3-amino, 1,2,4 aminotriazole precursor generated a nitrogen-rich mesoporous carbon nitride with a tri-s-triazine framework that achieved extended absorption in the visible region and a higher rate of H₂ evolution.^[25] In this case, nitrogen vacancy is more critical than the hydrogen bond.^[173,174] Therefore, the mechanism is still not very clear. More work is needed to reveal the working mechanisms.

3.3. Photonexcited Electron–Hole Utility

3.3.1. Heterostructures: Built-In Active Sites (Loading Cocatalysts)

Increasing the active sites is one effective strategy for enhancing HER photocatalytic activity. For carbon nitride, incorporating cocatalysts, catalyst anchoring, and enhancing surface area are practical approaches. In the case of lacking HER active sites on the surface, photodeposited Pt particles are the most commonly used cocatalysts for carbon nitrides in photocatalytic HER. However, due to the rarity and relatively high cost of platinum, Pt–carbon nitride is hard to commercialize. Other efficient HER cocatalysts are required to replace Pt, such as the emergent 2D materials, i.e., MoS₂, MXene, and transition metals.

MoS₂ can act as an efficient electrochemical HER agent.^[176,177] A MoS₂–carbon nitride heterostructure has demonstrated superior performance in photocatalytic HER. MoS₂ edge provides a large number of active sites for hydrogen evolution. In addition, the band alignment also shows that MoS₂ is an electron acceptor when it forms the heterostructure of carbon nitride, and photoexcited electrons are motivated by the difference of conduction bands to transfer from carbon nitride to the active sites on MoS₂. As shown in **Figure 13a,b**, sulfur atoms build electron transfer tunnels between MoS₂ and carbon nitride for efficient electron transport, and therefore, photoexcited electrons and holes are separated spatially. This case is slightly different from the PN junction discussed in the previous section: MoS₂ alone is almost photoinactive. Hence, there is no photoexcited holes transfer.^[175] In another work, the hydrogen production rate of Mo–Mo₂C/g-C₃N₄ heterojunction could reach 90% of that of 0.5 wt% Pt/g-C₃N₄. The superior HER performance of Mo–Mo₂C/g-C₃N₄ heterojunction benefits from both heterojunction properties and built-in active sites.^[178]

Well-designed transition metal particles decorated g-C₃N₄ based heterostructure also result in superior photocatalytic HER activity. The photocatalytic hydrogen evolution rate of 2 wt% nickel nanoparticles covered by graphene on g-C₃N₄ is 88 times higher than pure g-C₃N₄ and even better than that of 2 wt% Pt decorated g-C₃N₄. The enhancement of hydrogen generation rate is ascribed to active sites provided by Ni atoms and the unique structure of Ni@graphene, which offers efficient electron transfer and suppresses reverse reaction.^[137] Cobalt is also considered a potential substitute for Pt in photocatalytic HER.^[136] Cobalt nanoparticles embedded in carbon nanotube/carbon nitride heterostructure show superior performance compared with pristine carbon nitride. Providing a path for electrons from carbon nanotubes to reach the active

sites is also a way to enhance charge mobility, as discussed in Section 3.2.3.

3.3.2. Catalysts Distribution and Anchor Sites (Structure Change for More Cocatalyst Loading)

As discussed in the above paragraph, catalysts such as noble metals or transition metals are incorporated with carbon nitride to improve the catalytic activity. As Pt is the most frequently used cocatalyst in photocatalysis, here we give an example to discuss the status of Pt deposition on the photocatalysis performance of carbon nitride. Lau et al.^[107] observed that, by introducing urea moiety into the melon (i.e., g-C₃N₄), the hydrogen production rate was enhanced around 28 times, and the apparent quantum efficiency at 400 nm was increased by 36 times, compared to the counterpart without urea moiety. TEM image shows that Pt particles are evenly distributed on the surface of urea-derived CN (Figure 13d); meanwhile, melon without functionalization by a urea moiety suffers from aggregation (Figure 13c). Additionally, theoretical calculations show that urea moieties on melon can guide photogenerated charge into Pt particles, which boosts the hydrogen evolution rate. This result can also explain the superior performance of melon-based catalysts prepared from urea to those from dicyandiamide and melamine.^[107]

Pt particle aggregation and larger particle sizes can result in reduced Pt efficiency; apparently, the carbon nitride samples with single platinum atoms can have the highest Pt utilization rate. In addition, single-atom catalysts can achieve extraordinarily high performance in HER.^[179,180] However, the loading concentration of single atoms is usually very low, which depends on the number of active anchor sites and the surface area of different samples. Once the platinum loading amount exceeds the limitation, platinum clusters or nanoparticles will form on the surface instead of single atoms. Although the hydrogen evolution rate will keep increasing with the extra Pt after the limitation, the normalized hydrogen evolution rate versus Pt loading keeps decreasing.^[19,181] Single-atom doped carbon nitride for hydrogen evolution has been widely investigated, including noble metal and transition metals anchored on carbon nitride, which has been studied extensively for various applications, including HER.^[182–184]

Recently, researchers found that the coordination of a single nitrogen atom in carbon-based materials strongly influences the photocatalytic reaction activity.^[185–187] Xiao et al. fabricated a single copper atom doped carbon nitride, and the single copper atom formed Cu–N₃ and Cu–N₄ mixed configuration.^[185] The doped C₃N₄ exhibited strongly enhanced hydrogen evolution. The anchor sites also significantly affect the hydrogen generation performance. Jiang et al. fabricated Ag single-atom doped carbon nitride with Ag–N₂ and Ag–N₄ configurations.^[187] Experimental results indicated that Ag–N₂ anchored configuration demonstrated much better performance for hydrogen generation than the Ag–N₄ configuration. The difference of anchor sites may induce the variation of bandgap structure, charge carrier kinetics, and improvement in conductivity, which lead to the enhancement of HER performance, whereas the exact mechanism is not very clear since these variations may be different due to the diverse nature of various materials. More work needs to be done to understand the mechanisms.

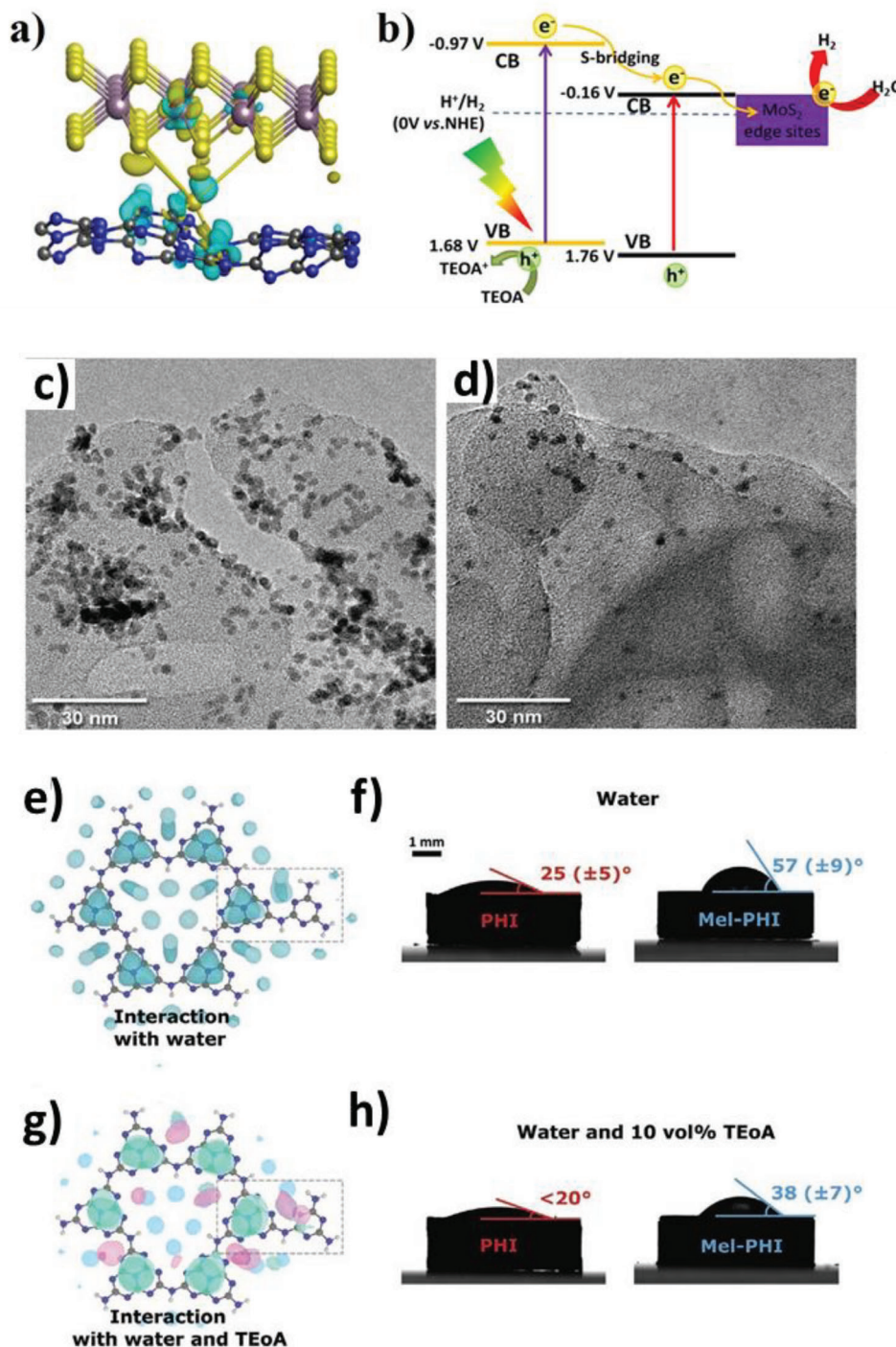


Figure 13. a) Charge density diagram of mesoporous CN/MoS₂ heterostructure. The yellow and navy regions represent net electron accumulation and depletion, respectively. The black, blue, yellow, and purple spheres are C, N, S, and Mo atoms, respectively. b) Proposed schematic diagram of the possible charge separation/transfer behavior for photocatalytic H₂ evolution under visible light irradiation. Reproduced with permission.^[175] Copyright 2019, Elsevier. c) TEM images of melon and d) melon-urea after photocatalytic reaction, showing the photodeposited platinum clusters as dark spots. Reproduced with permission.^[107] Copyright 2017, Wiley-VCH. e) Interaction of the melamine-PHI model system with water molecules. Blue areas depict the interaction of water molecules with the melamine-PHI model system. f) Contact angle measurement images of PHI (left) and melamine -PHI (right) with water after 30 s of equilibration time. g) Interaction of melamine -PHI model system with TEOA and water. Blue areas depict the interaction of water with the melamine -PHI model system, green areas the N atoms of TEOA, and red areas the OH groups, which interact strongly with the melamine group in Mel-PHI. h) The contact angle measurement images with water containing 10 vol% TEOA. Reproduced with permission.^[110] Copyright 2020, Wiley-VCH.

3.3.3. Surface and 3d Structure Design

A straightforward strategy to increase the number of intrinsic active sites and anchoring sites for catalysts (i.e., noble or transition metals) toward hydrogen evolution is to increase the surface area by introducing microstructures into photocatalysts. Developing a 3D structured photocatalyst will increase the surface area and the light absorption ability by trapping and reflecting the incident light within the interconnected 3D network.^[188] Carbon nitride photocatalysts with 3D macropores with a surface area of 40 m² g⁻¹ can double the hydrogen production rate compared with the counterpart in bulk with a limited surface area of less than 5 m² g⁻¹.^[189] To further increase the unit surface area and construct nanoporous structures, templates with ordered structures are typically used in the synthesis process.^[60,63,190–195] Templates can generally be cataloged into two streams: hard and soft templates. Since we are focusing on the effects caused by morphological and structural engineering, we are not going to discuss the properties and advantages of each type of template. On the other hand, to increase the surface area, layered carbon nitride can be made into nanosheets by exfoliation^[62,65,196] or nanostructured particles via thermal calcination.^[67,197]

As we mentioned at the beginning of Section 3.1.1, in most cases, the bandgap of carbon nitrides is broadened when the size of carbon nitrides is reduced. Hence the enlarged bandgap is a side effect when carbon nitrides are synthesized into nanoporous structures or in a nanosheet state to increase the unit surface area. In addition, narrow channels in nanosheet structure can allow oligomerization but inhibit polymerization of some precursors at 350 °C, such as melamine, resulting in a disturbed pyrolysis process and poor crystallinity.^[63] Despite enlarged bandgaps or poor crystallinity caused by the reduced dimensions of carbon nitride structures, the overall photocatalytic performance can still be enhanced because of the dramatically enlarged surface area, short migration distance of exciting charges and light-trapping ability.^[60,61,63,198,199] Therefore, control of crystal structure, morphology, and dimensions is always effective for enhancing the HER performance.

A list of carbon nitrides by controlling these parameters is summarized in Table 4. From the table, it can be seen that nanospherical g-C₃N₄ demonstrated the highest HER rate. The spherical carbon nitride is formed by g-C₃N₄ nanosheet, providing a large surface area and many shape edges and hence inducing a large number of active sites for HER.^[60] Another high-performance material is the spongy g-C₃N₄.^[61] The porous nature provides a high surface area and many channels for the transportation of water molecules for water splitting. Note that sophisticated nanostructured carbon nitrides could suffer from low permeability because of reduced channel size. The flow rate of the media solution in a small gap channel is lower than that in a large gap channel. For a given porosity, the permeability of porous substances decreases monotonously with increasing specific surface area according to liquid flow behaviors simulation in porous media.^[200] The lowered flow rate in small gap channels could also hinder hole scavengers from accessing active sites, thus promoting electron–hole recombination; produced hydrogen molecules could also accumulate in nanochannels to form bubbles, which can completely block channels from the media solution flowing through. The porous structure possesses sufficient channels for

molecular diffusion. Therefore, when designing a carbon nitride structure for high-performance water splitting, one must balance the high surface area (reduced size) and ion diffusion channels.

3.3.4. The Hydrophobic or Hydrophilic Property

Hydrophilicity and hydrophobicity are essential properties of the catalysts' surface, which strongly influence the HER performance. Introducing functional groups to graphitic carbon nitride can change not only the band structure but also the physical properties of the surface.^[110] For example, a hydrophilic surface could lead to the enhancement performance of HER since the water can more easily access to the active surface of the catalyst. Phosphorus (P) doped carbon nitride shows better hydrophilic properties due to the negatively charged surface, and its photocatalytic HER activity is actually increased.^[205] The band structure is optimized: a lower conduction band potential with a smaller bandgap (Figure 14a), and the conductivity is improved, evidenced by the EIS measurement as shown in Figure 14b. On the other hand, the introduction of P promoted the surface electronegativity, thus leading to the enhancement of affinity between materials and water molecules. The contact angle reduced from 40.3° to 24.3° after replacing corner site C atoms with P atoms in g-C₃N₄. Better hydrophilicity is beneficial for absorbing reactant molecules, reducing the size of gas bubbles, and shortening the time for the gas bubbles to stay around the catalyst, thus facilitating gas diffusion and leading to performance enhancement.^[106,206]

Another example is the oxygen plasma treatment of catalyst surface, in which –OH groups can be formed on the carbon nitride surface, which gives the treated sample an excellent dispersing performance in aqueous solutions ascribed to the hydrophilic nature of –OH groups.^[207] The oxygen plasma-modified carbon nitride also has a lower impedance and better photocatalytic performance in pollutant degradation.^[208] Therefore, the engineering of hydrophilicity and hydrophobicity may be a good strategy for enhancing HER performance,^[209,210] whereas how to combine and balance them in the catalysts to achieve both advantages is of challenge, and further work is needed to explore the mechanisms.

3.3.5. Hole Scavenger: Reverse Hole Transfer Effect

The reverse hole transfer (RHT) process could dominate the photocatalytic HER rate by influencing the hole-scavenging efficiency. The RHT process is illustrated in Figure 14c. Briefly, after a scavenger molecule captures a photoexcited hole, it will trigger the scavenger's reaction or be transferred back to the catalysts. As a frequently used hole scavenger (methanol), the RHT process of methanol/g-C₃N₄ has been studied by the femtosecond time-resolved transient absorption spectroscopy (fs-TA). According to the results, the RHT process of methanol/g-C₃N₄ takes 411 ps, 2.2 times and 1.3 times longer than ethylene glycol/g-C₃N₄ and ethanol/g-C₃N₄, respectively. The chance of HER for methanol/g-C₃N₄ will be higher. The prolonged RHT process explains that methanol is superior to both ethanol and ethylene glycol as the hole scavenger.^[205]

The hole scavenger effect on photocatalytic performance has also been investigated in other photocatalytic reactions.^[211] For

Table 4. Summary of crystallinity, structure, and conductivity effect on the HER.

	Enhancement (times)	H ₂ evolution rate [$\mu\text{mol h}^{-1}$]	Quantum efficiency	Light source	Refs.
Crystal structure					
Highly crystallized polytriazine imide 100 mg		189 (O ₂ evolution: 91)	8% at 365 nm	300 W Xe lamp $\lambda > 300$ nm	[77]
Hydrogen bond broken g-C ₃ N ₄ 50 mg	35	30		300 W Xe lamp $\lambda > 440$ nm	[171]
Highly crystallized g-C ₃ N ₄ 50 mg	7.8	38.6		300 W Xe lamp $\lambda > 420$ nm	[149]
Structural distortion g-C ₃ N ₄ 50 mg	2.4	58.1		300 W Xe lamp $\lambda > 420$ nm	[201]
Morphology					
Amorphous spongy g-C ₃ N ₄ 100 mg	170	203.5	6.1% at 420 nm	300 W Xe lamp $\lambda > 420$ nm	[61]
Nano-spherical g-C ₃ N ₄ 40 mg	46	574	9.6% at 420 nm	300 W Xe lamp $\lambda > 420$ nm	[60]
Vine-like g-C ₃ N ₄ 10 mg	38	135.6	12.7% at 420 nm	300 W Xe lamp $\lambda > 420$ nm	[198]
Torus g-C ₃ N ₄ 10 mg	34.9	0.4		400 W R7S lamp	[66]
MnO _x + porous g-C ₃ N ₄ 50 mg	18	53		300 W Xe lamp $\lambda > 420$ nm	[191]
Ultrathin g-C ₃ N ₄ 50 mg	7.8	40.6		300 W Xe lamp $\lambda > 420$ nm	[62]
g-C ₃ N ₄ aerogels 50 mg	7.5	30	3.1% at 420 nm	300 W Xe lamp $\lambda > 420$ nm	[199]
Double shelled g-C ₃ N ₄ 50 mg	6.7	27.5	1.2% at 420 nm	300 W Xe lamp $\lambda > 420$ nm	[63]
g-C ₃ N ₄ nanosheets 50 mg	6.5	169.5	11.3% at 405 nm	300 W Xe lamp $\lambda > 400$ nm	[196]
g-C ₃ N ₄ nanorods 25 mg	5.7	18.3		300 W Xe lamp $\lambda > 420$ nm	[64]
Onion-ring-like g-C ₃ N ₄ 10 mg	5	19		300 W Xe lamp $\lambda > 420$ nm	[192]
Tunable morphology g-C ₃ N ₄ 50 mg	4.9	3.21		50 W white LED array	[202]
Porous g-C ₃ N ₄ 15 mg	4	27.2	3.2% at 405 nm	50 W LED array $\lambda > 410$ nm	[203]
g-C ₃ N ₄ nanosheets 20 mg	4	16.7		300 W Xe lamp $\lambda > 420$ nm	[65]
Porous g-C ₃ N ₄ nanosheets 50 mg	3.7	155	74% at 400 nm	300 W Xe lamp $\lambda > 400$ nm	[197]
Polydopamine + nanospherical g-C ₃ N ₄ 30 mg	3	37.7		300 W Xe lamp $\lambda > 420$ nm	[190]
g-C ₃ N ₄ quantum dots 50 mg	3	5.75		300 W Xe lamp $\lambda > 420$ nm	[204]
Porous g-C ₃ N ₄ 10 mg	2.84	29		300 W Xe lamp $\lambda > 420$ nm	[189]
Mesoporous g-C ₃ N ₄ 100 mg		267		300 W Xe lamp $\lambda > 420$ nm	[193]

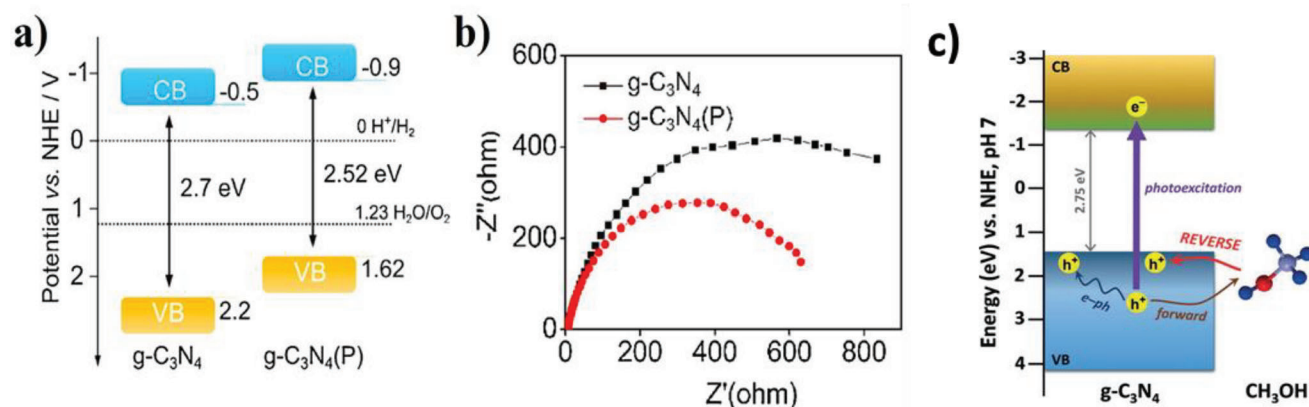


Figure 14. Illustration a) band structures for g-C₃N₄ and g-C₃N₄(P). b) EIS of g-C₃N₄ and g-C₃N₄(P). Reproduced with permission.^[106] Copyright 2018, Elsevier. c) Illustration of photogenerated hole dynamics at the CH₃OH/g-C₃N₄ interface. Reproduced with permission.^[205] Copyright 2018, Wiley-VCH.

example, Amal's group used different scavengers, including sucrose, acetic acid, salicylic acid, formic acid, methanol, and ethanol, for the photocatalytic reduction of selenium anions and discovered that formic acid showed the best performance. In contrast, sucrose, acetic acid, and salicylic acid did not induce photocatalytic activity,^[212] indicating that the choice of the appropriate hole scavengers may also be an effective strategy to enhance HER.

4. Conclusion, Challenges, and Prospective

4.1. Conclusions

In this review, we have discussed the mechanism and strategies for improving the photocatalytic HER performance of carbon nitride-based materials, composites, and heterojunctions. To overcome the relatively weak conductivity, conductive materials, such as carbon, graphene, and carbon nanotubes, are integrated with carbon nitride to enhance the charge transfer. In addition, incorporation with metallic catalysts, doping, and defects engineering have been widely employed for improving the catalytic activity. Bandgap engineering is used to enlarge the light absorption range, increase the active sites, and enhance the charge kinetics. Moreover, heterojunction formation is the most effective way to improve photocatalytic performance by enhancing light absorption, charge separation, and carrier photocatalysis activity.

On the other hand, materials synthesis and treatment are also critical in improving the performance of HER. The crystallinity, exposed facet of the nanocrystals, surface hydrophilicity, hydrogen content in the materials, and the selection of hole scavenger strongly influence the performance of photocatalytic HER.

4.2. Challenges and Perspectives

Though significant progress has been achieved in developing high-performance photocatalysts for HER, there is still a long journey toward commercialization. There are still problems and challenges in implementing the applications.

First, the noble metals such as Pt are usually used as a cocatalyst for HER, which is not the cost-effective system,^[213] while

the recycling technique of Pt is still not satisfying. Other low-cost metallic or non-metallic catalysts cannot achieve the desired efficiency for hydrogen generation. Recently, promising results have been extensively demonstrated, while there is still a long way to commercialization. Single-atom catalyst may be one of the promising candidates to reduce Pt usage and enhance the utilization, but efforts are needed to increase the concentration of single atom in the photocatalyst and to solve the stability issues.

Second, the mechanism of photocatalytic HER is still not very clear. Since several parameters influence the HER performance, it is not easy to have a clear picture of the underlying mechanism. For example, as discussed previously, the creation of nitrogen defects is accompanied by enhanced surface area, but it is difficult to determine which factor dominates performance enhancement.^[66,76,82] Delicate design of experiment is needed to clarify the photocatalytic HER mechanisms, which will further facilitate the development of high-performance catalytic systems. For example, ion implantation technique may be used for creating nitrogen vacancies without enhancing nanostructure surface areas. Hydrophilicity of the photocatalyst surface on the HER performance needs to be further investigated. Though there are various solutions and scavengers as well as catalysts, the major materials should have detailed parameters for optimizing the performance of hydrogen evolution by balancing hydrophilic and hydrophobic surface. Simulation and calculations should be employed to investigate the effect.^[214] Heterostructure with PN junction or Z-scheme has been one of the most effective approaches to achieve high-performance hydrogen evolution.^[215,216] New structures/schemes have been proposed, such as S-scheme and M scheme etc., whereas the mechanisms are still unclear. For example, it argues that Z-scheme heterostructure possesses higher photocatalysis activity than the conventional heterostructure. However, some works have reported high performance for PN junction. Detailed study and delicate design should be considered for investigating the mechanism. Due to the complicated morphology and structures of carbon nitrides, special design for building carbon nitride nanosheets with other materials to form PN junction or Z-scheme should be employed, thus reducing the influence of surface morphology and area during comparison. Certainly, machine learning and simulations are ideal tools for understanding the mechanisms. As discussed previously, most

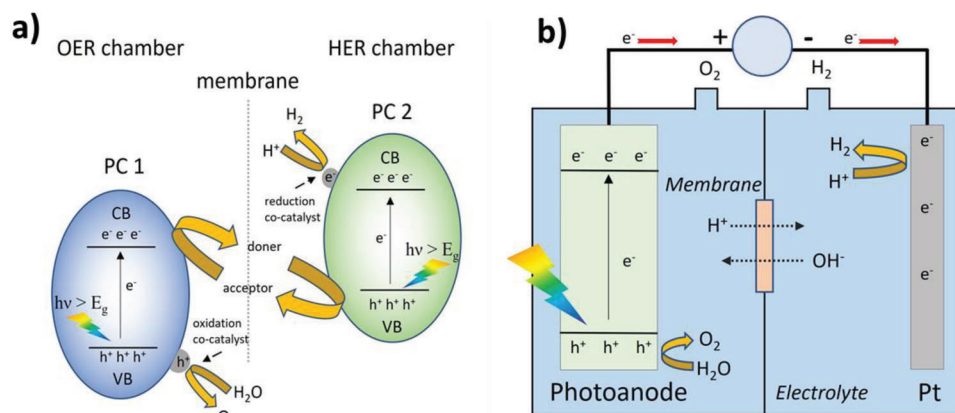


Figure 15. Illustration of a) schematic diagram of spatially separated OER and HER. b) Schematic diagram of HER system with a membrane in the photoelectrochemical reaction.

of the carbon nitride can only absorb light near UV. Most of the visible light cannot be utilized. In the future work, multilayered catalyst similar to that of solar cell^[217] rather than PN junction or Z scheme can also be a possible way to absorb more visible light, excite electrons and holes, enhance electron/hole separation, kinetics, and catalytic activities.^[218]

Third, achieving optimized composites, heterostructure, or photocatalysis cell is complicated. Different research groups reported various performances with the same material, which may be related to their synthesis method, parameters control, and optimized integration of hydrogen production cell, etc. For example, the hydrogen evolution rates of two unmodified carbon nitride samples prepared by urea are 4365 and 457.8 $\mu\text{mol h}^{-1} \text{g}^{-1}$, respectively, which is one magnitude difference. The measured results cannot be compared directly. Then the enhancement of their modified counterparts can be noted as 8.6 and 2 times, respectively.^[76,106] Therefore, it is difficult to understand the mechanism and fundamental factors influencing photocatalysis and also difficult to confirm which is correct. Besides the delicate design of the experiment setup, a standard measurement system for issuing the certificate should be proposed like the efficiency of solar cells.

To realize the commercialization of photocatalysis, upon the strategies discussed in this review, efforts are needed to be made to developing new materials for high-performance photocatalytic reactions. Noble metal like Pt electrode/catalysts should be substituted by other low-cost and abundant elements/compounds to reduce the cost. For example, recently, MoS_2 as the cocatalyst has demonstrated promising potential,^[175] whereas, the performance is still lower than that of Pt. Developing new materials should be one of the keys for solving the issue. Many catalysts have shown better performance than standard Pt electrode, though stability needs significant improvement. As discussed previously, many parameters may influence the performance of hydrogen evolution, it may be challenging to design ideal experiment for directly investigating the factors individually, such as the catalysts' crystallinity, surface area, defects and functional groups and how to balance and optimize these parameters for maximizing the catalytic activity of advanced nanomaterials becomes an extremely difficult task. Therefore, theoretical calculations plus

machine learning may be used to simulate different conditions for photocatalytic reactions. The screening of hundreds of materials may be a possible way to search for high-performance photocatalysts, which cannot be carried out by experimental work.

The ideal case for achieving a high-performance photocatalytic device toward hydrogen production is that the catalyst materials possess an extensive range of spectrum absorption. The photoexcited electrons/holes immediately participate in a reaction or with a short charge transfer path. To avoid charge carriers recombination, HER and OER should occur at different locations. In this case, we conceptualize a two-chamber system with a membrane, as shown in **Figure 15a**. The difficulty for this system is the unidirectional charge diffusion in the membrane and fast charge kinetics of the electrons and holes. A small electric potential is applied to the anode and cathode to improve further the device performance similar to the photoelectrochemical system, which will facilitate the charge transport, as shown in **Figure 15b**. In this design, a nanostructured semiconductor can also replace the Pt electrode. Optimizing the applied potential, semiconductor bandgap, membrane, and electrolyte may lead to a high-performance photocatalytic reaction. Certainty, the qualified membrane, and the optimization of the HER system are the barriers to practical applications.

Acknowledgements

J.Y. acknowledges the financial support by ARC Future Fellowship (FT160100205) and DP220103045. J.-H.Y., A.V. and J.Y. thank for the financial support from the National Research Foundation of Korea and funded by the Ministry of Science, ICT, and Future Planning (Grant No.: 2022K1A4a8A01080312).

Open access publishing facilitated by The University of Newcastle, as part of the Wiley - The University of Newcastle agreement via the Council of Australian University Librarians.

Conflict of Interest

The authors declare no conflict of interest.

Keywords

carbon nitride, hydrogen evolution reaction, photocatalysis

Received: April 6, 2023

Revised: May 27, 2023

Published online: June 12, 2023

- [1] P. Selvarajan, M. Fawaz, C. Sathish, M. Y. Li, D. W. Chu, X. J. Yu, M. B. H. Breese, J. B. Yi, A. Vinu, *Adv. Energy Sustainability Res.* **2021**, 2, 2100104.
- [2] Y. Goto, T. Hisatomi, Q. Wang, T. Higashi, K. Ishikiriyama, T. Maeda, Y. Sakata, S. Okunaka, H. Tokudome, M. Katayama, S. Akiyama, H. Nishiyama, Y. Inoue, T. Takewaki, T. Setoyama, T. Minegishi, T. Takata, T. Yamada, K. Domen, *Joule* **2018**, 2, 509.
- [3] M. D. Ji, J. L. Wang, *Int. J. Hydrogen Energy* **2021**, 46, 38612.
- [4] I. Dincer, C. Acar, *Int. J. Hydrogen Energy* **2015**, 40, 11094.
- [5] M. Tawalbeh, A. Al-Othman, F. Kafiah, E. Abdelsalam, F. Almomani, M. Alkasrawi, *Sci. Total Environ.* **2021**, 759, 143528.
- [6] G. Kothandam, G. Singh, X. Guan, J. M. Lee, K. Ramadass, S. Joseph, M. Benzigar, A. Karakoti, J. Yi, P. Kumar, A. Vinu, *Adv. Sci.* **2023**, e2301045.
- [7] M. Li, P. Selvarajan, S. Wang, T. Wan, S. Xi, X. Wang, J. Xue, S. C. Indirathankam, X. Geng, L. Qiao, A. Vinu, D. Chu, J. Yi, *Small Struct.* **2023**, 2300010.
- [8] C. Marchal, T. Cottineau, M. G. Mendez-Medrano, C. Colbeau-Justin, V. Caps, V. Keller, *Adv. Energy Mater.* **2018**, 8, 1702142.
- [9] H. S. Gujral, G. Singh, A. V. Baskar, X. Guan, X. Geng, A. V. Kotkondawar, S. Rayalu, P. Kumar, A. Karakoti, A. Vinu, *Sci. Technol. Adv. Mater.* **2022**, 23, 76.
- [10] A. Fujishima, K. Honda, *Nature* **1972**, 238, 37.
- [11] H. Nishiyama, T. Yamada, M. Nakabayashi, Y. Maehara, M. Yamaguchi, Y. Kuromiya, Y. Nagatsuma, H. Tokudome, S. Akiyama, T. Watanabe, R. Narushima, S. Okunaka, N. Shibata, T. Takata, T. Hisatomi, K. Domen, *Nature* **2021**, 598, 304.
- [12] S. Ali, S. Ali, P. M. Ismail, H. Shen, A. Zada, A. Ali, I. Ahmad, R. Shah, I. Khan, J. Chen, C. Cui, X. Wu, Q. Kong, J. Yi, X. Zu, H. Xiao, F. Raziq, L. Qiao, *Appl. Catal., B* **2022**, 307, 121149.
- [13] M. Li, Z. Zhou, L. Hu, S. Wang, Y. Zhou, R. Zhu, X. Chu, A. Vinu, T. Wan, C. Cazorla, J. Yi, D. Chu, *ACS Appl. Mater. Interfaces* **2022**, 14, 16338.
- [14] H. S. Gujral, M. Fawaz, S. Joseph, C. I. Sathish, G. Singh, X. J. Yu, M. B. H. Breese, J. B. Yi, M. Singh, V. Bansal, A. Karakoti, A. Vinu, *ACS Appl. Nano Mater.* **2022**, 5, 12077.
- [15] X. Chu, C. I. Sathish, M. Li, J. H. Yang, W. Li, D. C. Qi, D. Chu, A. Vinu, *J. Yi, Battery Energy* **2023**, 2, 20220041.
- [16] H. S. Gujral, G. Singh, J. H. Yang, C. I. Sathish, J. B. Yi, A. Karakoti, M. Fawaz, K. Ramadass, A. H. Al-Muhtaseb, X. J. Yu, M. B. H. Breese, A. Vinu, *Carbon* **2022**, 195, 9.
- [17] R. H. Shah, S. Ali, F. Raziq, S. Ali, P. M. Ismail, S. Y. Shah, R. Iqbal, X. Q. Wu, W. D. He, X. T. Zu, A. Zada, Adnan, F. Mabood, A. Vinu, S. H. Jhung, J. B. Yi, L. Qiao, *Coord. Chem. Rev.* **2023**, 477, 214968.
- [18] A. V. Baskar, G. Singh, A. M. Ruban, J. M. Davidraj, R. Bahadur, P. Sooriyakumar, P. Kumar, A. Karakoti, J. B. Yi, A. Vinu, *Adv. Funct. Mater.* **2023**, 33, 2208349.
- [19] L. Zhang, R. Long, Y. Zhang, D. Duan, Y. Xiong, Y. Zhang, Y. Bi, *Angew. Chem., Int. Ed.* **2020**, 59, 6224.
- [20] Z. H. Lei, J. M. Lee, G. Singh, C. I. Sathish, X. Z. Chu, A. H. Al-Muhtaseb, A. Vinu, J. B. Yi, *Energy Storage Mater.* **2021**, 36, 514.
- [21] G. Singh, K. Ramadass, V. D. B. C. DasiReddy, X. Z. Yuan, Y. S. Ok, N. Bolan, X. Xiao, T. Y. Ma, A. Karakoti, J. B. Yi, A. Vinu, *Prog. Mater. Sci.* **2023**, 135, 101104.
- [22] J. M. Lee, P. Selvarajan, S. Kim, G. Singh, S. Joseph, J.-H. Yang, J. Yi, A. Vinu, *Nano Energy* **2021**, 90, 106602.
- [23] W. J. Ong, L. L. Tan, Y. H. Ng, S. T. Yong, S. P. Chai, *Chem. Rev.* **2016**, 116, 7159.
- [24] M. Ismael, Y. Wu, *Sustainable Energy Fuels* **2019**, 3, 2907.
- [25] G. P. Mane, S. N. Talapaneni, K. S. Lakhi, H. Ilbeygi, U. Ravon, K. Al-Bahily, T. Mori, D. H. Park, A. Vinu, *Angew. Chem., Int. Ed.* **2017**, 56, 8481.
- [26] C. I. Sathish, G. Kothandam, P. Selvarajan, Z. Lei, J. Lee, J. Qu, A. H. Al-Muhtaseb, X. Yu, M. B. H. Breese, R. Zheng, J. Yi, A. Vinu, *Adv. Sci.* **2022**, 9, 2105603.
- [27] C. I. Sathish, S. Premkumar, X. Chu, X. Yu, M. B. H. Breese, M. Al-Abri, A. H. Al-Muhtaseb, A. Karakoti, J. Yi, A. Vinu, *Angew. Chem., Int. Ed.* **2021**, 60, 21242.
- [28] J. Mee Lee, S. Joseph, I. Chirchir Bargarora, S. Kim, G. Singh, J. H. Yang, K. Ramadass, R. Bahadur, X. Yu, M. Bh Breese, J. Yi, A. Vinu, *Batteries Supercaps* **2022**, 5, 202100369.
- [29] A. Hayat, A. G. Al-Sehemi, K. S. El-Nasser, T. A. Taha, A. A. Al-Ghamdi, J. A. S. Syed, M. A. Amin, T. Ali, T. Bashir, A. Palamanit, J. Khan, W. I. Nawawi, *Int. J. Hydrogen Energy* **2022**, 47, 5142.
- [30] S. M. Ruban, G. Singh, K. Ramadass, S. Joseph, A. Ismaili, C.-Y. Huang, X. Guan, P. Kumar, Y. Sugi, A. Vinu, *ChemCatChem* **2023**, 202300240.
- [31] K. Qi, Y. Xie, R. Wang, S.-y. Liu, Z. Zhao, *Appl. Surf. Sci.* **2019**, 466, 847.
- [32] S. Liang, Z. Wang, Z. Zhou, G. Liang, Y. Zhang, *Biosens. Bioelectron.* **2022**, 217, 114370.
- [33] J. Oh, J. M. Lee, Y. Yoo, J. Kim, S. J. Hwang, S. Park, *Appl. Catal., B* **2017**, 218, 349.
- [34] Q. Xiang, J. Yu, M. Jaroniec, *J. Phys. Chem. C* **2011**, 115, 7355.
- [35] X. Guan, Z. Li, X. Geng, Z. Lei, A. Karakoti, T. Wu, P. Kumar, J. Yi, A. Vinu, *Small* **2023**, 19, e2207181.
- [36] C. Zhu, X. Chen, J. Ma, C. Gu, Q. Xian, T. Gong, C. Sun, *J. Phys. Chem. C* **2018**, 122, 20444.
- [37] J. Jiang, Z. Xiong, H. Wang, G. Liao, S. Bai, J. Zou, P. Wu, P. Zhang, X. Li, *J. Mater. Sci. Technol.* **2022**, 118, 15.
- [38] C. M. Li, H. H. Wu, D. Q. Zhu, T. X. Zhou, M. Yan, G. Chen, J. X. Sun, G. Dai, F. Ge, H. J. Dong, *Appl. Catal., B* **2021**, 297, 120433.
- [39] F. Raziq, A. Hayat, M. Humayun, S. K. B. Mane, M. B. Faheem, A. Ali, Y. Zhao, S. B. Han, C. Cai, W. Li, D. C. Qi, J. B. Yi, X. J. Yu, M. B. H. Breese, F. Hassan, F. Ali, A. Mavlonov, K. Dhanabalan, X. Xiang, X. T. Zu, S. Li, L. Qiao, *Appl. Catal., B* **2020**, 270, 118867.
- [40] Y. H. Bai, Y. J. Zheng, Z. Wang, Q. Hong, S. Q. Liu, Y. F. Shen, Y. J. Zhang, *New J. Chem.* **2021**, 45, 11876.
- [41] L. Cheng, H. Zhang, X. Li, J. Fan, Q. Xiang, *Small* **2021**, 17, 2005231.
- [42] Z. Zhou, Y. Zhang, Y. Shen, S. Liu, Y. Zhang, *Chem. Soc. Rev.* **2018**, 47, 2298.
- [43] V. R. Battula, S. Kumar, D. K. Chauhan, S. Samanta, K. Kailasam, *Appl. Catal., B* **2019**, 244, 313.
- [44] W. J. Jiang, Q. S. Ruan, J. J. Xie, X. J. Chen, Y. F. Zhu, J. W. Tang, *Appl. Catal., B* **2018**, 236, 428.
- [45] T. Wu, P. Wang, J. Qian, Y. Ao, C. Wang, J. Hou, *Dalton Trans.* **2017**, 46, 13793.
- [46] L. Zhou, H. Y. Zhang, H. Q. Sun, S. M. Liu, M. O. Tade, S. B. Wang, W. Q. Jin, *Catal. Sci. Technol.* **2016**, 6, 7002.
- [47] M. Ismael, *J. Alloys Compd.* **2020**, 846, 156446.
- [48] S. N. Talapaneni, G. Singh, I. Y. Kim, K. AlBahily, A. H. Al-Muhtaseb, A. S. Karakoti, E. Tavakkoli, A. Vinu, *Adv. Mater.* **2020**, 32, 1904635.
- [49] G. Singh, J. Lee, A. Karakoti, R. Bahadur, J. Yi, D. Zhao, K. AlBahily, A. Vinu, *Chem. Soc. Rev.* **2020**, 49, 4360.
- [50] M. Kaur, K. Singh, A. Vij, A. Kumar, *New J. Chem.* **2023**, 47, 2137.
- [51] M. Pourmadadi, E. Rahmani, M. M. Eshaghi, A. Shamsabadipour, S. Ghotekar, A. Rahdar, L. F. R. Ferreira, *J. Drug Delivery Sci. Technol.* **2023**, 79, 104001.

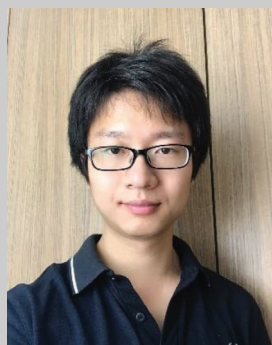
- [52] Q. Wang, Y. Li, F. Huang, S. Song, G. Ai, X. Xin, B. Zhao, Y. Zheng, Z. Zhang, *Molecules* **2023**, *28*, 432.
- [53] A. V. Zhurenok, D. B. Vasilchenko, E. A. Kozlova, *Int. J. Mol. Sci.* **2023**, *24*, 346.
- [54] A. Kumar, P. Raizada, A. Hosseini-Bandegharai, V. K. Thakur, V. Nguyen, P. Singh, *J. Mater. Chem. A* **2021**, *9*, 111.
- [55] G. F. Liao, Y. Gong, L. Zhang, H. Y. Gao, G. J. Yang, B. Z. Fang, *Environ. Sci.* **2019**, *12*, 2080.
- [56] R. Malik, V. K. Tomer, *Renewable Sustainable Energy Rev.* **2021**, *135*, 110235.
- [57] N. Rono, J. K. Kibet, B. S. Martincigh, V. O. Nyamori, *Crit. Rev. Solid State Mater. Sci.* **2020**, *46*, 189.
- [58] J. L. Wang, S. Z. Wang, *Coord. Chem. Rev.* **2022**, *453*, 214338.
- [59] X. W. Ruan, X. Q. Cui, G. R. Jia, J. D. Wu, J. X. Zhao, D. J. Singh, Y. H. Liu, H. Y. Zhang, L. Zhang, W. T. Zheng, *Chem. Eng. J.* **2022**, *428*, 132579.
- [60] J. Zhang, M. Zhang, C. Yang, X. Wang, *Adv. Mater.* **2014**, *26*, 4121.
- [61] M. Z. Rahman, P. C. Tapping, T. W. Kee, R. Smernik, N. Spooner, J. Moffatt, Y. H. Tang, K. Davey, S. Z. Qiao, *Adv. Funct. Mater.* **2017**, *27*, 201702384.
- [62] C. C. Dong, Z. Y. Ma, R. T. Qie, X. H. Guo, C. H. Li, R. J. Wang, Y. L. Shi, B. Dai, X. Jia, *Appl. Catal., B* **2017**, *217*, 629.
- [63] L. Luo, K. Y. Li, A. F. Zhang, H. N. Shi, G. H. Zhang, J. N. Ma, W. Zhang, J. W. Tang, C. S. Song, X. W. Guo, *J. Mater. Chem. A* **2019**, *7*, 17815.
- [64] Y. X. Zeng, X. Liu, C. B. Liu, L. L. Wang, Y. C. Xia, S. Q. Zhang, S. L. Luo, Y. Pei, *Appl. Catal., B* **2018**, *224*, 1.
- [65] H. N. Che, L. H. Liu, G. B. Che, H. J. Dong, C. B. Liu, C. M. Li, *Chem. Eng. J.* **2019**, *357*, 209.
- [66] I. Papailias, N. Todorova, T. Giannakopoulou, N. Ioannidis, P. Dallas, D. Dimotikali, C. Trapalis, *Appl. Catal., B* **2020**, *268*, 118733.
- [67] Y. Wang, P. Du, H. Pan, L. Fu, Y. Zhang, J. Chen, Y. Du, N. Tang, G. Liu, *Adv. Mater.* **2019**, *31*, 1807540.
- [68] P. Niu, M. Qiao, Y. F. Li, L. Huang, T. Y. Zhai, *Nano Energy* **2018**, *44*, 73.
- [69] J. Tian, L. Zhang, M. Wang, X. Jin, Y. Zhou, J. Liu, J. Shi, *Appl. Catal., B* **2018**, *232*, 322.
- [70] X. Q. Fan, L. X. Zhang, R. L. Cheng, M. Wang, M. L. Li, Y. J. Zhou, J. L. Shi, *ACS Catal.* **2015**, *5*, 5008.
- [71] X. Q. Fan, L. X. Zhang, M. Wang, W. M. Huang, Y. J. Zhou, M. L. Li, R. L. Cheng, J. L. Shi, *Appl. Catal., B* **2016**, *182*, 68.
- [72] H. Ou, X. Chen, L. Lin, Y. Fang, X. Wang, *Angew. Chem., Int. Ed.* **2018**, *57*, 8729.
- [73] J. Liu, Y. Yu, R. L. Qi, C. Y. Cao, X. Y. Liu, Y. J. Zheng, W. G. Song, *Appl. Catal., B* **2019**, *244*, 459.
- [74] S. Chu, Y. Wang, Y. Guo, J. Y. Feng, C. C. Wang, W. J. Luo, X. X. Fan, Z. G. Zou, *ACS Catal.* **2013**, *3*, 912.
- [75] M. K. Bhunia, K. Yamauchi, K. Takanebe, *Angew. Chem., Int. Ed.* **2014**, *53*, 11001.
- [76] Q. Han, Z. Cheng, B. Wang, H. Zhang, L. Qu, *ACS Nano* **2018**, *12*, 5221.
- [77] L. H. Lin, Z. Y. Lin, J. Zhang, X. Cai, W. Lin, Z. Y. Yu, X. C. Wang, *Nat. Catal.* **2020**, *3*, 649.
- [78] N. N. Meng, J. Ren, Y. Liu, Y. Huang, T. Petit, B. Zhang, *Environ. Sci.* **2018**, *11*, 566.
- [79] Z. Wei, M. L. Liu, Z. J. Zhang, W. Q. Yao, H. W. Tan, Y. F. Zhu, *Environ. Sci.* **2018**, *11*, 2581.
- [80] H. Li, Z. Liang, Q. Deng, W. Hou, *J. Colloid Interface Sci.* **2020**, *564*, 333.
- [81] V. Ragupathi, P. Panigrahi, N. G. Subramaniam, *Optik* **2020**, *202*, 163601.
- [82] H. C. Lan, L. L. Li, X. Q. An, F. Liu, C. B. Chen, H. J. Liu, J. H. Qu, *Appl. Catal., B* **2017**, *204*, 49.
- [83] B. Yang, J. Han, Q. Zhang, G. F. Liao, W. J. Cheng, G. X. Ge, J. C. Liu, X. D. Yang, R. J. Wang, X. Jia, *Carbon* **2023**, *202*, 348.
- [84] J. Xu, M. Fujitsuka, S. Kim, Z. Wang, T. Majima, *Appl. Catal., B* **2019**, *241*, 141.
- [85] C. F. Li, Y. F. Ji, Q. Y. Wei, Z. B. Liu, Y. Y. Wu, L. S. Chen, D. X. Han, L. Niu, C. L. Tao, D. D. Qin, *ACS Appl. Energy Mater.* **2023**, *6*, 997.
- [86] Y. H. Li, Z. J. He, L. Liu, Y. Jiang, W. J. Ong, Y. Y. Duan, W. K. Ho, F. Dong, *Nano Energy* **2023**, *105*, 108032.
- [87] X. Zhang, P. J. Ma, C. Wang, L. Y. Gan, X. J. Chen, P. Zhang, Y. Wang, H. Li, L. H. Wang, X. Y. Zhou, K. Zheng, *Environ. Sci.* **2022**, *15*, 830.
- [88] X. Li, J. Bai, J. Li, C. Li, X. Zhong, S. Deng, *RSC Adv* **2020**, *10*, 7019.
- [89] Y. Li, Z. Wang, T. Xia, H. Ju, K. Zhang, R. Long, Q. Xu, C. Wang, L. Song, J. Zhu, J. Jiang, Y. Xiong, *Adv. Mater.* **2016**, *28*, 6959.
- [90] S. C. Sun, G. Q. Shen, J. W. Jiang, W. B. Mi, X. L. Liu, L. Pan, X. W. Zhang, J. J. Zou, *Adv. Energy Mater.* **2019**, *9*, 201901505.
- [91] T. Tong, B. W. He, B. C. Zhu, B. Cheng, L. Y. Zhang, *Appl. Surf. Sci.* **2018**, *459*, 385.
- [92] X. Jin, R. Wang, L. Zhang, R. Si, M. Shen, M. Wang, J. Tian, J. Shi, *Angew. Chem., Int. Ed.* **2020**, *59*, 6827.
- [93] J.-W. Zhang, S. Gong, N. Mahmood, L. Pan, X. Zhang, J.-J. Zou, *Appl. Catal., B* **2018**, *221*, 9.
- [94] H. Lv, Y. Huang, R. T. Koodali, G. Liu, Y. Zeng, Q. Meng, M. Yuan, *ACS Appl. Mater. Interfaces* **2020**, *12*, 12656.
- [95] X. Guan, M. Fawaz, R. Sarkar, C.-H. Lin, Z. Li, Z. Lei, P. D. Nithinraj, P. Kumar, X. Zhang, J.-H. Yang, *J. Mater. Chem. A* **2023**, <https://doi.org/10.1039/D3TA00318C>.
- [96] Z. A. Lan, G. G. Zhang, X. C. Wang, *Appl. Catal., B* **2016**, *192*, 116.
- [97] L. F. Gao, T. Wen, J. Y. Xu, X. P. Zhai, M. Zhao, G. W. Hu, P. Chen, Q. Wang, H. L. Zhang, *ACS Appl. Mater. Interfaces* **2016**, *8*, 617.
- [98] L. Luo, Z. Y. Gong, J. N. Ma, K. R. Wang, H. X. Zhu, K. Y. Li, L. Q. Xiong, X. W. Guo, J. W. Tang, *Appl. Catal., B* **2021**, *284*, 119742.
- [99] J. Yao, D. Liu, B. Zhao, Y. Zhou, L. Y. Zhang, T. Peng, *J. Photochem. Photobiol., A* **2023**, *436*, 114359.
- [100] X. Xiao, Y. Gao, L. Zhang, J. Zhang, Q. Zhang, Q. Li, H. Bao, J. Zhou, S. Miao, N. Chen, J. Wang, B. Jiang, C. Tian, H. Fu, *Adv. Mater.* **2020**, *32*, 2003082.
- [101] B. Yue, Q. Li, H. Iwai, T. Kako, J. Ye, *Sci. Technol. Adv. Mater.* **2011**, *12*, 034401.
- [102] Y. Y. Shang, Y. J. Ma, X. Chen, X. Xiong, J. Pan, *Mol. Catal.* **2017**, *433*, 128.
- [103] W. Wu, Z. Ruan, J. Li, Y. Li, Y. Jiang, X. Xu, D. Li, Y. Yuan, K. Lin, *Nano-Micro Lett.* **2019**, *11*, 10.
- [104] R. J. Qi, P. F. Yu, J. C. Zhang, W. Q. Guo, Y. Y. He, H. Hojo, H. Einaga, Q. Zhang, X. S. Liu, Z. Jiang, W. F. Shangguan, *Appl. Catal., B* **2020**, *274*, 119099.
- [105] Y. J. Si, Y. J. Zhang, L. H. Lu, S. Zhang, Y. Chen, J. H. Liu, H. Y. Jin, S. E. Hou, K. Dai, W. G. Song, *Appl. Catal., B* **2018**, *225*, 512.
- [106] B. Wang, H. R. Cai, D. M. Zhao, M. Song, P. H. Guo, S. H. Shen, D. S. Li, S. C. Yang, *Appl. Catal., B* **2019**, *244*, 486.
- [107] V. W. H. Lau, V. W. Z. Yu, F. Ehrat, T. Botari, I. Moudrakovski, T. Simon, V. Duppel, E. Medina, J. K. Stolarczyk, J. Feldmann, V. Blum, B. V. Lotsch, *Adv. Energy Mater.* **2017**, *7*, 201602251.
- [108] Z. Y. Fang, Y. J. Bai, L. H. Li, D. Li, Y. Y. Huang, R. J. Chen, W. Q. Fan, W. D. Shi, *Nano Energy* **2020**, *75*, 104865.
- [109] K. Schwinghammer, B. Tuffy, M. B. Mesch, E. Wirnhier, C. Martineau, F. Taulelle, W. Schnick, J. Senker, B. V. Lotsch, *Angew. Chem. Int. Ed.* **2013**, *52*, 2435.
- [110] J. Kröger, A. Jiménez-Solano, G. Savasci, P. Rovó, I. Moudrakovski, K. Küster, H. Schlöberg, H. A. Vignolo-González, V. Duppel, L. Grunenberg, C. B. Dayan, M. Sitti, F. Podjaski, C. Ochsenfeld, B. V. Lotsch, *Adv. Energy Mater.* **2020**, *11*, 2003016.
- [111] A. Gołębiewska, M. P. Kobylański, A. Zaleska-Medynska, in *Metal Oxide-Based Photocatalysis: Fundamentals and Prospects for Application*, (Ed.: A. Zaleska-Medynska), Elsevier, Amsterdam **2018**, p. 3.

- [112] F. Raziq, L. Q. Sun, Y. Y. Wang, X. L. Zhang, M. Humayun, S. Ali, L. L. Bai, Y. Qu, H. T. Yu, L. Q. Jing, *Adv. Energy Mater.* **2018**, *8*, 1701580.
- [113] X. J. She, J. J. Wu, H. Xu, J. Zhong, Y. Wang, Y. H. Song, K. Q. Nie, Y. Liu, Y. C. Yang, M. T. F. Rodrigues, R. Vajtai, J. Lou, D. L. Du, H. M. Li, P. M. Ajayan, *Adv. Energy Mater.* **2017**, *7*, 1700025.
- [114] S. W. Cao, X. F. Liu, Y. P. Yuan, Z. Y. Zhang, Y. S. Liao, J. Fang, S. C. J. Loo, T. C. Sum, C. Xue, *Appl. Catal., B* **2014**, *147*, 940.
- [115] Q. L. Xu, L. Y. Zhang, B. Cheng, J. J. Fan, J. G. Yu, *Chem* **2020**, *6*, 1543.
- [116] D. E. Lee, K. P. Reddy, S. Moru, W. K. Jo, S. Tonda, *Appl. Surf. Sci.* **2023**, *610*, 155569.
- [117] X. Li, Q. Luo, L. Han, F. Deng, Y. Yang, F. Dong, *J. Mater. Sci. Technol.* **2022**, *114*, 222.
- [118] D. M. Zhao, Y. Q. Wang, C. L. Dong, Y. C. Huang, J. Chen, F. Xue, S. H. Shen, L. J. Guo, *Nat. Energy* **2021**, *6*, 388.
- [119] Y. Z. Wu, W. Xu, W. C. Tang, Z. K. Wang, Y. Wang, Z. X. Lv, Y. Zhang, W. Zhong, H. L. Cai, R. S. Yang, X. S. Wu, *Nano Energy* **2021**, *90*, 106532.
- [120] Z. F. Huang, J. J. Song, X. Wang, L. Pan, K. Li, X. W. Zhang, L. Wang, J. J. Zou, *Nano Energy* **2017**, *40*, 308.
- [121] W. Chen, Z. C. He, G. B. Huang, C. L. Wu, W. F. Chen, X. H. Liu, *Chem. Eng. J.* **2019**, *359*, 244.
- [122] W. Chang, W. Xue, E. Liu, J. Fan, B. Zhao, *Chem. Eng. J.* **2019**, *362*, 392.
- [123] Y.-C. Nie, F. Yu, L.-C. Wang, Q.-J. Xing, X. Liu, Y. Pei, J.-P. Zou, W.-L. Dai, Y. Li, S. L. Suib, *Appl. Catal., B* **2018**, *227*, 312.
- [124] E. V. Pean, S. Dimitrov, C. S. De Castro, M. L. Davies, *Phys. Chem. Chem. Phys.* **2020**, *22*, 28345.
- [125] X. Chen, J. Wang, Y. Chai, Z. Zhang, Y. Zhu, *Adv. Mater.* **2021**, *33*, 2007479.
- [126] W. Li, X. Wang, M. Li, S. A. He, Q. Ma, X. C. Wang, *Appl. Catal., B* **2020**, *268*, 118384.
- [127] K. T. Wong, S. C. Kim, K. Yun, C. E. Choong, I. W. Nah, B. H. Jeon, Y. Yoon, M. Jang, *Appl. Catal., B* **2020**, *273*, 119034.
- [128] W. Yu, J. Chen, T. Shang, L. Chen, L. Gu, T. Peng, *Appl. Catal., B* **2017**, *219*, 693.
- [129] X. Y. Jiang, Z. Y. Zhang, M. H. Sun, W. Z. Liu, J. D. Huang, H. Y. Xu, *Appl. Catal., B* **2021**, *281*, 119473.
- [130] Z. Q. Gao, K. Y. Chen, L. Wang, B. Bai, H. Liu, Q. Z. Wang, *Appl. Catal., B* **2020**, *268*, 118462.
- [131] L. Y. Kunz, B. T. Diroll, C. J. Wrasman, A. R. Riscoe, A. Majumdar, M. Cargnello, *Environ. Sci.* **2019**, *12*, 1657.
- [132] Y. Tan, Z. Shu, J. Zhou, T. Li, W. Wang, Z. Zhao, *Appl. Catal., B* **2018**, *230*, 260.
- [133] G. Zhou, M.-F. Wu, Q.-J. Xing, F. Li, H. Liu, X.-B. Luo, J.-P. Zou, J.-M. Luo, A.-Q. Zhang, *Appl. Catal., B* **2018**, *220*, 607.
- [134] Y. Ma, J. Li, E. Liu, J. Wan, X. Hu, J. Fan, *Appl. Catal., B* **2017**, *219*, 467.
- [135] W. Che, W. Cheng, T. Yao, F. Tang, W. Liu, H. Su, Y. Huang, Q. Liu, J. Liu, F. Hu, Z. Pan, Z. Sun, S. Wei, *J. Am. Chem. Soc.* **2017**, *139*, 3021.
- [136] Q. X. Liu, C. M. Zeng, Z. H. Xie, L. H. Ai, Y. Y. Liu, Q. Zhou, J. Jiang, H. Q. Sun, S. B. Wang, *Appl. Catal., B* **2019**, *254*, 443.
- [137] L. J. Fang, X. L. Wang, Y. H. Li, P. F. Liu, Y. L. Wang, H. D. Zeng, H. G. Yang, *Appl. Catal., B* **2017**, *200*, 578.
- [138] X. J. Bai, R. L. Zong, C. X. Li, D. Liu, Y. F. Liu, Y. F. Zhu, *Appl. Catal., B* **2014**, *147*, 82.
- [139] Q. Han, B. Wang, J. Gao, L. Qu, *Angew. Chem., Int. Ed.* **2016**, *55*, 10849.
- [140] W. Xing, C. Li, G. Chen, Z. Han, Y. Zhou, Y. Hu, Q. Meng, *Appl. Catal., B* **2017**, *203*, 65.
- [141] L. Q. Kong, Y. J. Ji, Z. Z. Dang, J. Q. Yan, P. Li, Y. Y. Li, S. Z. Liu, *Adv. Funct. Mater.* **2018**, *28*, 201800668.
- [142] K. C. Christoforidis, Z. Syrgiannis, V. La Parola, T. Montini, C. Petit, E. Stathatos, R. Godin, J. R. Durrant, M. Prato, P. Fornasiero, *Nano Energy* **2018**, *50*, 468.
- [143] E. S. Da Silva, N. M. M. Moura, M. G. P. M. S. Neves, A. Coutinho, M. Prieto, C. G. Silva, J. L. Faria, *Appl. Catal., B* **2018**, *221*, 56.
- [144] S. P. Adhikari, Z. D. Hood, H. Wang, R. Peng, A. Krall, H. Li, V. W. Chen, K. L. More, Z. L. Wu, S. Geyer, A. Lachgar, *Appl. Catal., B* **2017**, *217*, 448.
- [145] X. B. Dong, H. Wang, X. L. Li, P. Fatehi, S. J. Wang, Q. Wu, K. Y. Liu, F. G. Kong, *Appl. Surf. Sci.* **2023**, *610*, 155570.
- [146] J. F. Du, Y. L. Shen, F. Yang, J. L. Wei, K. H. Xu, X. N. Li, C. H. An, *Appl. Surf. Sci.* **2023**, *608*, 155199.
- [147] X. Yang, Y. Zhang, J. Deng, X. Huo, Y. Wang, R. Jia, *Catalysts* **2023**, *13*, 139.
- [148] J. J. Liu, W. Fu, Y. L. Liao, J. J. Fan, Q. J. Xiang, *J. Mater. Sci. Technol.* **2021**, *91*, 224.
- [149] J. S. Cheng, Z. Hu, K. L. Lv, X. F. Wu, Q. Li, Y. H. Li, X. F. Li, J. Sun, *Appl. Catal., B* **2018**, *232*, 330.
- [150] J. Ma, X. X. Peng, Z. X. Zhou, H. Yang, K. Q. Wu, Z. Z. Fang, D. Han, Y. F. Fang, S. Q. Liu, Y. F. Shen, Y. J. Zhang, *Angew. Chem., Int. Ed. Engl.* **2022**, *61*, 202210856.
- [151] S. W. Yang, W. Li, C. C. Ye, G. Wang, H. Tian, C. Zhu, P. He, G. Q. Ding, X. M. Xie, Y. Liu, Y. Lifshitz, S. T. Lee, Z. H. Kang, M. H. Jiang, *Adv. Mater.* **2017**, *29*, 1605625.
- [152] I. Y. Kim, S. Kim, X. Y. Jin, S. Premkumar, G. Chandra, N. S. Lee, G. P. Mane, S. J. Hwang, S. Umopathy, A. Vinu, *Angew. Chem., Int. Ed. Engl.* **2018**, *57*, 17135.
- [153] G. Zhou, Y. Shan, Y. Hu, X. Xu, L. Long, J. Zhang, J. Dai, J. Guo, J. Shen, S. Li, L. Liu, X. Wu, *Nat. Commun.* **2018**, *9*, 3366.
- [154] H. Yang, Z. Wang, S. Q. Liu, Y. F. Shen, Y. J. Zhang, *Chin. Chem. Lett.* **2020**, *31*, 3047.
- [155] J. Mahmood, E. K. Lee, M. Jung, D. Shin, H. J. Choi, J. M. Seo, S. M. Jung, D. Kim, F. Li, M. S. Lah, N. Park, H. J. Shin, J. H. Oh, J. B. Baek, *Proc. Natl. Acad. Sci. USA* **2016**, *113*, 7414.
- [156] G. P. Mane, S. N. Talapaneni, K. S. Lakhi, H. Ilbeygi, U. Ravon, K. Al-Bahily, T. Mori, D. H. Park, A. Vinu, *Angew. Chem., Int. Ed.* **2017**, *56*, 8481.
- [157] P. Kumar, E. Vahidzadeh, U. K. Thakur, P. Kar, K. M. Alam, A. Goswami, N. Mahdi, K. Cui, G. M. Bernard, V. K. Michaelis, K. Shankar, *J. Am. Chem. Soc.* **2019**, *141*, 5415.
- [158] Z. L. Zhao, Z. Shu, J. Zhou, T. T. Li, F. Yan, W. B. Wang, L. A. Xu, L. L. Shi, Z. H. Liao, *J. Alloys Compd.* **2022**, *910*, 164828.
- [159] J. N. Zhao, L. Ma, H. Y. Wang, Y. F. Zhao, J. Zhang, S. Z. Hu, *Appl. Surf. Sci.* **2015**, *332*, 625.
- [160] R. Y. Zhang, A. L. Zhang, Y. H. Cao, S. Y. Wang, F. Dong, Y. Zhou, *Chem. Eng. J.* **2020**, *401*, 126028.
- [161] F. Raziq, J. X. He, J. T. Gan, M. Humayun, M. B. Faheem, A. Iqbal, A. Hayat, S. Fazal, J. B. Yi, Y. Zhao, K. Dhanabalan, X. Q. Wu, A. Mavlonov, T. Ali, F. Hassan, X. Xiang, X. T. Zu, H. H. Shen, S. A. Li, L. Qiao, *Appl. Catal., B* **2020**, *270*, 118870.
- [162] H. Bao, L. Wang, G. Li, L. Zhou, Y. Xu, Z. Liu, M. H. Wu, *Carbon* **2021**, *179*, 80.
- [163] M. Aleksandrak, W. Kukulka, E. Mijowska, *Appl. Surf. Sci.* **2017**, *398*, 56.
- [164] A. Du, S. Sanvito, Z. Li, D. Wang, Y. Jiao, T. Liao, Q. Sun, Y. H. Ng, Z. Zhu, R. Amal, S. C. Smith, *J. Am. Chem. Soc.* **2012**, *134*, 4393.
- [165] A. Yuan, H. Lei, F. Xi, J. Liu, L. Qin, Z. Chen, X. Dong, *J. Colloid Interface Sci.* **2019**, *548*, 56.
- [166] Y. P. Zhu, T. Z. Ren, Z. Y. Yuan, *ACS Appl. Mater. Interfaces* **2015**, *7*, 16850.
- [167] B. Liu, L. Ye, R. Wang, J. Yang, Y. Zhang, R. Guan, L. Tian, X. Chen, *ACS Appl. Mater. Interfaces* **2018**, *10*, 4001.

- [168] L. B. Jiang, X. Z. Yuan, G. M. Zeng, X. H. Chen, Z. B. Wu, J. Liang, J. Zhang, H. Wang, H. Wang, *ACS Sustainable Chem. Eng.* **2017**, 5, 5831.
- [169] C. Y. Liu, Y. H. Zhang, F. Dong, A. H. Reshak, L. Q. Ye, N. Pinna, C. Zeng, T. R. Zhang, H. W. Huang, *Appl. Catal., B* **2017**, 203, 465.
- [170] W. H. Wang, X. Kou, T. Li, R. G. Zhao, Y. G. Su, *J. Photochem. Photobiol., A* **2023**, 435, 114308.
- [171] Y. Kang, Y. Yang, L. C. Yin, X. Kang, L. Wang, G. Liu, H. M. Cheng, *Adv. Mater.* **2016**, 28, 6471.
- [172] X. D. Kang, Y. Y. Kang, X. X. Hong, Z. H. Sun, C. Zhen, C. H. Hu, G. Liu, H. M. Cheng, *Prog. Nat. Sci.: Mater. Int.* **2018**, 28, 183.
- [173] C. Cheng, J. Shi, L. Wen, C.-L. Dong, Y.-C. Huang, Y. Zhang, S. Zong, Z. Diao, S. Shen, L. Guo, *Carbon* **2021**, 181, 193.
- [174] Y. Zhang, Z. Huang, C.-L. Dong, J. Shi, C. Cheng, X. Guan, S. Zong, B. Luo, Z. Cheng, D. Wei, Y.-c. Huang, S. Shen, L. Guo, *Chem. Eng. J.* **2022**, 431, 134101.
- [175] G. Dong, P. Qiu, F. Y. Meng, Y. Wang, B. He, Y. S. Yu, X. Q. Liu, Z. Li, *Chem. Eng. J.* **2020**, 384, 123330.
- [176] M. Y. Li, B. H. Cai, R. M. Tian, X. J. Yu, M. B. H. Breese, X. Z. Chu, Z. J. Han, S. Li, R. Joshi, A. Vinu, T. Wan, Z. M. Ao, J. B. Yi, D. W. Chu, *Chem. Eng. J.* **2021**, 409, 128158.
- [177] M. Y. Li, Y. C. Kuo, X. Z. Chu, D. W. Chu, J. B. Yi, *Emergent Mater.* **2021**, 4, 579.
- [178] J. Dong, Y. Shi, C. Huang, Q. Wu, T. Zeng, W. Yao, *Appl. Catal., B* **2019**, 243, 27.
- [179] Z. H. Lei, C. I. Sathish, Y. P. Liu, A. Karokoti, J. Wang, L. Qiao, A. Vinu, J. B. Yi, *EcoMat* **2022**, 4, e12186.
- [180] F. Wahid, S. Ali, P. M. Ismail, F. Raziq, S. Ali, J. Yi, L. Qiao, *Prog. Energy* **2022**, 5, 012001.
- [181] Y. Q. Zhu, T. Wang, T. Xu, Y. X. Li, C. Y. Wang, *Appl. Surf. Sci.* **2019**, 464, 36.
- [182] B. Yu, H. Li, J. White, S. Donne, J. Yi, S. Xi, Y. Fu, G. Henkelman, H. Yu, Z. Chen, T. Ma, *Adv. Funct. Mater.* **2019**, 30, 1905665.
- [183] S. K. Kaiser, Z. Chen, D. Faust Akl, S. Mitchell, J. Perez-Ramirez, *Chem. Rev.* **2020**, 120, 11703.
- [184] A. Q. Wang, J. Li, T. Zhang, *Nat. Rev. Chem.* **2018**, 2, 65.
- [185] X. Xiao, Y. Gao, L. Zhang, J. Zhang, Q. Zhang, Q. Li, H. Bao, J. Zhou, S. Miao, N. Chen, J. Wang, B. Jiang, C. Tian, H. Fu, *Adv. Mater.* **2020**, 32, 2003082.
- [186] G. Liu, H. Lv, Y. Zeng, M. Yuan, Q. Meng, Y. Wang, C. Wang, *Trans. Tianjin Univ.* **2021**, 27, 139.
- [187] X. H. Jiang, L. S. Zhang, H. Y. Liu, D. S. Wu, F. Y. Wu, L. Tian, L. L. Liu, J. P. Zou, S. L. Luo, B. B. Chen, *Angew. Chem., Int. Ed.* **2020**, 59, 23112.
- [188] J. H. Yang, S. Kim, I. Y. Kim, J. M. Lee, J. B. Yi, A. Karakoti, S. Joseph, K. Albahily, A. Vinu, *Sustainable Mater. Technol.* **2020**, 25, e00184.
- [189] Q. Liang, Z. Li, X. Yu, Z. H. Huang, F. Kang, Q. H. Yang, *Adv. Mater.* **2015**, 27, 4634.
- [190] H. Wang, Q. Lin, L. Yin, Y. Yang, Y. Qiu, C. Lu, H. Yang, *Small* **2019**, 15, 1900011.
- [191] M. H. Ai, J. W. Zhang, R. J. Gao, L. Pan, X. W. Zhang, J. J. Zou, *Appl. Catal., B* **2019**, 256, 117805.
- [192] L. Cui, J. Song, A. F. McGuire, S. Kang, X. Fang, J. Wang, C. Yin, X. Li, Y. Wang, B. Cui, *ACS Nano* **2018**, 12, 5551.
- [193] G. P. Mane, S. N. Talapaneni, K. S. Lakhi, H. Ilbeygi, U. Ravon, K. Al-Bahily, T. Mori, D. H. Park, A. Vinu, *Angew. Chem., Int. Ed.* **2017**, 56, 8481.
- [194] F. Guo, Z. H. Chen, Y. X. Shi, L. W. Cao, X. F. Cheng, W. L. Shi, L. Z. Chen, X. Lin, *Renewable Energy* **2022**, 188, 1.
- [195] D. Liu, C. L. Li, C. Y. Zhao, Q. Zhao, T. Q. Niu, L. K. Pan, P. W. Xu, F. Q. Zhang, W. D. Wu, T. J. Ni, *Chem. Eng. J.* **2022**, 438, 135623.
- [196] P. Yang, H. Ou, Y. Fang, X. Wang, *Angew. Chem., Int. Ed.* **2017**, 56, 3992.
- [197] D. Ruan, S. Kim, M. Fujitsuka, T. Majima, *Appl. Catal., B* **2018**, 238, 638.
- [198] Y. Zhang, L. L. Wu, X. Y. Zhao, Y. N. Zhao, H. Q. Tan, X. Zhao, Y. Y. Ma, Z. Zhao, S. Y. Song, Y. H. Wang, Y. G. Li, *Adv. Energy Mater.* **2018**, 8, 201801139.
- [199] H. Ou, P. Yang, L. Lin, M. Anpo, X. Wang, *Angew. Chem. Int. Ed.* **2017**, 56, 10905.
- [200] Y. P. Chen, C. Q. Shen, P. F. Lu, Y. P. Huang, *Chem. Eng. Process.* **2015**, 87, 104.
- [201] L. Zeng, X. Ding, Z. Z. Sun, W. M. Hua, W. L. Song, S. Y. Liu, L. M. Huang, *Appl. Catal., B* **2018**, 227, 276.
- [202] A. Savateev, S. Pronkin, J. D. Epping, M. G. Willinger, M. Antonietti, D. Dontsova, *J. Mater. Chem. A* **2017**, 5, 8394.
- [203] J. Barrio, A. Grafmuller, J. Tzadikov, M. Shalom, *Appl. Catal., B* **2018**, 237, 681.
- [204] X. J. Bai, S. C. Yan, J. J. Wang, L. Wang, W. J. Jiang, S. L. Wu, C. P. Sun, Y. F. Zhu, *J. Mater. Chem. A* **2014**, 2, 17521.
- [205] Z. Chen, Q. Zhang, Y. Luo, *Angew. Chem., Int. Ed.* **2018**, 57, 5320.
- [206] B. K. Kim, M. J. Kim, J. J. Kim, *ACS Appl. Mater. Interfaces* **2021**, 13, 11940.
- [207] X. Bu, J. Li, S. Yang, J. Sun, Y. Deng, Y. Yang, G. Wang, Z. Peng, P. He, X. Wang, G. Ding, J. Yang, X. Xie, *ACS Appl. Mater. Interfaces* **2016**, 8, 31419.
- [208] X. Ji, X. Yuan, J. Wu, L. Yu, H. Guo, H. Wang, H. Zhang, D. Yu, Y. Zhao, *ACS Appl. Mater. Interfaces* **2017**, 9, 24616.
- [209] K. Alam, Y. Sim, J. H. Yu, J. Gnanaprakasam, H. Choi, Y. Chae, U. Sim, H. Cho, *Materials* **2020**, 13, 12.
- [210] S. Tanaka, S. Takaya, T. Kumeda, N. Hoshi, K. Miyatake, M. Nakamura, *Int. J. Hydrogen Energy* **2021**, 46, 28078.
- [211] N. Denisov, J. Yoo, P. Schmuki, *Electrochim. Acta* **2019**, 319, 61.
- [212] T. Tan, D. Beydoun, R. Amal, *J. Photochem. Photobiol., A* **2003**, 159, 273.
- [213] Y. L. Xie, Y. Cui, D. J. Wu, Y. K. Zeng, L. L. Sun, *Int. J. Hydrogen Energy* **2021**, 46, 27841.
- [214] B. H. Jing, Z. M. Ao, Z. Y. Teng, C. Y. Wang, J. B. Yi, T. C. An, *Sustainable Mater. Technol.* **2018**, 16, 12.
- [215] H. X. Shi, D. C. Feng, H. M. Li, D. S. Yu, X. D. Chen, *J. Photochem. Photobiol., A* **2023**, 435, 114292.
- [216] M. Wang, S. Xu, Z. Ge, Y. Li, Z. Zhou, Y. Chen, *Ind. Eng. Chem. Res.* **2023**, 62, 961.
- [217] X. Che, Y. Li, Y. Qu, S. R. Forrest, *Nat. Energy* **2018**, 3, 422.
- [218] G. F. Liao, C. X. Li, X. Z. Li, B. Z. Fang, *Cell Rep. Phys. Sci.* **2021**, 2, 100355.



C.I. Sathish is working as a research associate at the University of Newcastle, Australia. He received his Ph.D. from Hokkaido University, Japan, and worked as a post-doctoral fellow at NIMS, Japan, and continuingly he joined Seoul National University as IBS fellow in the Center for Correlated Electron Systems. His research areas include the synthesis of novel materials, studying their structural, electronic, magnetic, and superconducting properties, the design and development of multifunctional nanoporous materials such as mesoporous and microporous carbon nitrides, carbon, hybrid inorganic materials, metal carbonitrides for energy storage, sensors, CO₂ capture and conversion, catalysis, and environmental applications.



Xinwei Guan is currently a postdoctoral fellow at University of Newcastle. He received his Ph.D. degree in materials science & engineering from the University of New South Wales (UNSW, Australia) in 2021 and M.S. degree from King Abdullah University of Science and Technology (KAUST, Saudi Arabia) in 2017. His research focuses on halide-perovskite-based optoelectronics, including nonvolatile memories, transistors, and photodetectors. His research activities also include energy applications like solar cells, photothermal applications, and catalysis.



Xiangwei Zhang is a Ph.D. student in mineral processing engineering from China University of Mining and Technology (Beijing). He received his Bachelor's degree from China University of Mining and Technology (Beijing) in 2018. Currently, he is a visiting student at the University of Newcastle under the supervision of Prof. Ajayan Vinu. His research focuses on environmental mineral materials for wastewater treatment and carbon nitride-based materials for energy applications.



Jiabao Yi is an associate professor at the Global Innovative Center for Advanced Nanomaterials, School of Engineering, University of Newcastle, Australia. His research areas include magnetic semiconductors, ferromagnetism in 2D materials, soft/hard magnetic materials and their applications in spintronics, bioapplications, and environment applications as well as advanced electronic materials for clean energy production, energy storage and conversion, sensors, and carbon oxide capture and conversion.